ROYAUME DU MAROC
Université Mohammed V - RABAT -
جامعة محمد الخامس – الرباط –
Faculté des sciences
كلية العلوم
CENTRE D'ETUDES DOCTORALES - SCIENCES ET TECHNOLOGIES

N° d'ordre : 3405

THESE

En vue de l'obtention du : ***DOCTORAT***

Structure de Recherche : Laboratoire de la Matière Condensée et Sciences Interdisciplinaires (LaMCScI)
Discipline : Physique
Spécialité : Physique des Nanomatériaux

Présentée et soutenue le : 19/12/2020 par :

Mohamed TADOUT

Magnetocaloric effect in Gd-based alloy thin films and heterostructures

JURY

Abdelilah BENYOUSSEF	PES, Académie Hassan II des sciences et techniques-Rabat	Président
Mohammed BENAISSA	PES, Faculté des Sciences, Université Mohammed V-Rabat	Directeur de Thèse
Mohammed LOULIDI	PES, Faculté des Sciences, Université Mohammed V-Rabat	Rapporteur/ Examinateur
Hamid EZ-ZAHRAOUY	PES, Faculté des Sciences, Université Mohammed V-Rabat	Rapporteur/ Examinateur
Noureddine MASAIF	PES, Faculté des Sciences, Université Ibn Tofail- Kénitra	Rapporteur/ Examinateur
Mohamed BALLI	PES, Université Internationale de Rabat	Examinateur
Stéphane MANGIN	PES, Université de Lorraine -France	Examinateur
Omar MOUNKACHI	PA, Faculté des Sciences, Université Mohammed V-Rabat	Invité

Année Universitaire: 2019/2020

✉ Faculté des Sciences, avenue Ibn Battouta, BP. 1014 RP, Rabat –Maroc
☎ 00212(0) 37 77 18 76 🖷 00212(0) 37 77 42 61 ; http://www.fsr.ac.ma

Preamble

The work presented in this thesis was carried out at the laboratories:

- Laboratory of Condensed Matter and Interdisciplinary Sciences (LaMCScI) at the faculty of Sciences (Mohammed V University).
- Institut Jean Lamour (IJL) at the University of Lorraine.

The financial, scientific and technical support devoted to the realization of this thesis was provided by:

- Ministry of Higher Education, Scientific Research, and Professional Training (Enssup) (Morocco) and the National Center for Scientific and Technological Research (CNRST) through the grant Number: PPR/2015/57

Acknowledgments

This thesis has been carried out at "Laboratory of Condensed Matter and Interdisciplinary Sciences (LaMCScI)" Faculty of Sciences, Mohammed V University – Rabat, under the supervision of **Professor Mohammed BENAISSA**, and the co-supervision of **Professor Omar MOUNKACHI**

On this page, I would like to express my very great appreciation, deep gratitude and sincere thanks to my supervisor **Professor Mohammed BENAISSA**, for giving me this opportunity to learn from his valuable expertise and to have fruitful discussions with him. He always had time to answer my questions and he patiently provided the vision, encouragement and advice necessary for me to proceed throughout my research period. It is my privilege to be his student.

My sincere gratitude goes to **Professor Abdelilah BENYOUSSEF**, Member of the Hassan II Academy of Science and Technology who chaired the jury of the defense.

I would like to express my thanks to **Professor Mohammed LOULIDI**, from the Faculty of Science in Rabat, for reporting and reviewing this thesis.

I would like also to express my thanks to **Professor Hamid EZ-ZAHRAOUY**, from the Faculty of Science in Rabat, for reporting and reviewing this thesis.

I would like also to express my thanks to **Professor Noureddine MASAIF**, from the Faculty of Sciences, Ibn Tofail University- Kénitra, for reporting and reviewing this thesis.

I would like also to express my thanks to **Professor Mohamed BALLI,** From International University of Rabat, for reviewing this PhD thesis.

My deepest thanks go to **Professor. Stéphane MANGIN**, Professor at University of Lorraine and Head of the Spintronic and Nano-magnetism research team at the Institut Jean Lamour (IJL) at University of Lorraine, for allow me to perform an essential part of my thesis. I express my deep gratitude for his availability, his advice, and his great scientific culture of which he was kind enough to share with me during my stay in his lab.

I also warmly thank **Professor Omar MOUNKACHI**, from the Faculty of Science in Rabat, for his support. This work could not have been accomplished without his respective contribution, the fantastic discussions we had, and his sense of humor. I express my deepest gratitude to him for his kindness, his attentive listening, his efficiency and his availability along this work.

I would also like to thank all the technical and scientific staff from the LaMCScI Laboratory, all members and colleagues in Institut Jean Lamour, as well as in MAScIR Foundation, with whom I had a lot of fun working with on the fabrication and characterization of my samples.

I present my special thanks to my friends in Morocco , France, and USA (**Mohammed Salah el Hadri**) who constantly help me not only in research but also in many aspects of my life during my Ph.D study, though I can't list all of their names.

Finally, I would like to thanks my parents for their infinite and continuous support and patience. For always being there and help me through the harder moments. To my grand-mother for being an example, for being the source of love that never ends and for being the mother of us all. To my aunts, uncles and my cousins - thank you!

Abstract:

Magnetic refrigeration based on the magnetocaloric effect (MCE) is a promising alternative to conventional gas compression based cooling techniques. Understanding impacts of reduced dimensionality on the magnetocaloric response of a material such as Gadolinium (Gd) or its alloys is essential in optimizing the performance of cooling devices, which is also the overall goal of this thesis..

Most of the thesis work focuses on thin films and multilayers of $Gd_{100-x}Co_x$ alloys in which a magnetocaloric effect has been demonstrated and for which the industrial feasibility seems to be the most favorable. In a first step, the structural, magnetic and magnetocaloric properties of these alloys are explored and optimized. On the other hand, we are also interested in the influence of disorder on critical exponents and the magnetocaloric effect. The analysis shows that the critical exponents for $Gd_{100-x}Co_x$ are close to those of the mean field theory.

On the other hand, the multilayers stack of Gd-Co alloys with concentration and transition temperature (Tc) values is also studied. Thanks to this stacking of the multilayers the relative cooling capacity (RCP) can be increased compared to that of solid gadolinium. This study demonstrates the potential of Gd-Co multilayer stacking for magnetic cooling applications.

An exploratory section is devoted to thin films and multilayers of $Gd_{100-x}Tb_x$ alloys that could potentially have a workable magnetocaloric effect. The magnetic and structural transitions of these alloys of different compositions are studied and their potential for magnetocaloric application is discussed.

Keywords: Thin film, magnetocaloric effect, transition metals and rare earths alloy, magnetic refrigeration, magnetic.

Résumé :

La réfrigération magnétique basée sur l'effet magnétocalorique (MCE) est une alternative prometteuse aux techniques de refroidissement conventionnelles basées sur la compression des gaz. La compréhension des impacts de la nanostructuration sur la réponse magnétocalorique d'un matériau tel que le Gadolinium (Gd) ou ses alliages est essentielle pour optimiser les performances des dispositifs de refroidissement, ce qui est également l'objectif global de cette thèse.

La majeure partie des travaux de thèse se focalise sur les couches minces et les multicouches des alliages $Gd_{100-x}Co_x$ dans lesquels un effet magnétocalorique a été mis en évidence et pour lesquels la faisabilité industrielle semble la plus favorable. Dans un premier temps, les propriétés structurales, magnétiques et magnétocaloriques de ces alliages sont explorées et optimisées. D'autre part nous nous sommes aussi intéressés à l'influence du désordre sur les exposants critiques et à l'effet magnétocalorique. L'analyse montre que les exposants critiques pour $Gd_{100-x}Co_x$ sont proches à ceux de la théorie champ moyen.

D'autre part, les multicouches des alliages Gd-Co avec valeurs de concentration et de température de transition (Tc) est également étudié. Grâce à cet empilement des multicouches le pouvoir de refroidissement relatif (RCP) peut être augmenter par rapport à celle du gadolinium massif. Cette étude démontre le potentiel de l'empilement des multicouches de Gd-Co pour les applications de refroidissement magnétique

Un volet exploratoire est consacré aux couches minces et les multicouches des alliages $Gd_{100-x}Tb_x$ qui pourraient potentiellement avoir un effet magnétocalorique exploitable. Les transitions magnétiques et structurales de ces alliages de compositions différentes sont étudiées et leur potentiel d'application magnétocalorique est discuté.

Mots clés : Couches minces , effet magnétocalorique, alliages de métaux de transition et de terres rares, réfrigération magnétique, magnétisme.

Résumé détaillé :

La réfrigération magnétique est une technologie émergente et prometteuse qui pourrait constituer une alternative pour produire du froid avec une efficacité énergétique élevée et sans impact sur l'environnement. De plus en plus de prototypes ont été construits à travers le monde au cours de ces dix dernières années. Ils mettent en évidence la faisabilité de la technologie mais révèlent également des problèmes scientifiques et techniques qu‘il est nécessaire de maîtriser pour aboutir à un système réel performant. Nous avons défini la problématique en précisant les inconvénients de la réfrigération classique et nous avons présenté des alternatives de production de froid qui écartent l‘utilisation fluides frigorigènes polluants, puis nous avons montré l‘efficacité de la réfrigération magnétique qui est basée sur l‘effet magnétocalorique.

Dans cette thèse, les propriétés structurales, magnétiques et magnétocaloriques dans les couches minces et les hétérostructures à base de Gd ont été systématiquement explorées et optimisées. L'effet d’interface est également étudié.

Le but de ce travail de doctorat était de contribuer à une meilleure compréhension des caractéristiques fondamentales des couches minces magnétiques, en mettant l'accent sur la relation entre la modification de la composition et l'alternance dans les propriétés magnétiques et magnétocaloriques. Les principaux résultats de la thèse sont résumés comme ci-dessous :

Dans la première partie de cette thèse, des couches minces de composés d'alliage $Gd_{100-x}Co_x$ ont été déposées sur un substrat de silicium par des techniques de pulvérisation cathodique. L'effet magnétique et magnéto-calorique des couches minces de $Gd_{100-x}Co_x$ (x=44, 48, 52, 56) a été étudié. La température de Curie augmente lorsque la concentration de l'élément Cobalt augmente. Les variations maximales de l'entropie magnétique des échantillons ont atteint un maximum à la température de Curie. Sous un champ magnétique appliqué de 2 T, la valeur des variations d'entropie magnétique est de 2,64 pour x = 44, respectivement. De plus, les échantillons présentent une importante puissance de refroidissement relative "RCP" supérieure à 140 J/Kg qui est considérée comme un paramètre recommandé pour une large gamme de températures dans les applications de réfrigération magnétique. De plus, l'étude des propriétés

critiques de la transition ferromagnétique du second ordre du film mince de $Gd_{100-x}Co_x$ démontre que l'interaction magnétique autour de Tc peut être décrite avec le modèle de champ moyen correspondant à l'interaction à longue distance.

Dans ce contexte, nous avons démontré une approche efficace pour améliorer les propriétés magnétocaloriques des multicouches à base de Gd-Co. Nous avons vérifié que le multicouche de Gd-Co subit une transition de second ordre à la température de Curie. La valeur de $-\Delta S_M$ et RCP pour la multicouche à base d'alliage Gd-Co étudiée est comparée à celle obtenue pour les couches d'alliage Gd-Co individuelles. Les valeurs maximales de $-\Delta S_M$ pour le multicouche atteignent 1,54 $J.Kg^{-1}.K^{-1}$ pour un changement de champ magnétique de 0 à 20 kOe, ce qui est inférieur à celui obtenu pour n'importe quelle couche d'alliage de Gd-Co. Cependant, le pic $-\Delta S_M$ est beaucoup plus large pour le multicouche et la valeur RCP peut atteindre 200 J/Kg. Cette amélioration de la PCR démontre le potentiel des multicouches à base de Gd-Co pour les applications de réfrigération magnétique.

Enfin, nous avons démontré la possibilité de régler indépendamment la position et l'amplitude du pic de variation de l'entropie dans les systèmes Gd-Tb. La température de transition et les variations d'entropie magnétique des couches minces d'alliage $Gd_{100-x}Tb_x$ pourraient être réglés en modifiant la composition de l'alliage. De plus, nous démontrons que la fabrication des multicouches de [Gd/Tb] avec la même épaisseur et concentration des couches minces d'alliage $Gd_{100-x}Tb_x$ étudiés permet d'augmenter fortement la puissance de refroidissement relative (RCP), et d'atteindre des valeurs deux fois plus grandes que celles des alliages correspondants. Grâce à cette approche, la variation de l'entropie peut être contrôlée en continu à partir des propriétés individuelles de ses éléments constitutifs. Cette étude ouvre de nouvelles possibilités dans le contrôle et l'optimisation de l'effet magnétocalorique dans les couches minces magnétiques.

Table of Contents

List of Figures

List of Tables

List of Abbreviations

Abbreviation	Full name
MR	Magnetic refrigeration
MCE	Magnetocaloric effect
CFC	Chlorofluorocarbons
HCFC	Hydro Chlorofluorocarbons
XRD	X-ray diffraction
PPMS	Physical properties measurement system
FWHM	Full width at half maximum
RCP	Relative cooling power
FM	Ferromagnetic
FOMT	First order magnetic transition
SOMT	Second order magnetic transition
SQUID	Superconducting quantum device
PVD	Physical vapour deposition
ΔS_M	Magnetic entropy change
T_c	Curie temperature
ΔT_{ad}	Adiabatic Temperature change

General Introduction

The magnetocaloric effect (MCE) is a phenomenon that enables the temperature of a material to be altered by fields. The most broadly known example of the MCE is adiabatic demagnetization, which appears in most elementary statistical mechanics textbooks and has been used in ultralow temperature work for decades. The fairly recent surge of interest in the magnetocaloric effect was sparked by Pecharsky and Gschneidner's discovery of the giant MCE near room temperature in bulk $Gd_5(SixGe_{1-x})_4$.This made the prospect of commercializing magnetic cooling tenable. To this day, the primary technological motivation for MCE research is the development of highly efficient and environmentally friendly magnetic refrigeration near room temperature, which can be used for residential or commercial cooling (air conditioners, refrigerators, and freezers), and more industrial purposes such as gas liquefaction (perhaps further from room temperature). The impact of developing cost-effective magnetic refrigeration at room temperature would literally be global.

Exploration of the large MCE and RCP in magnetic materials on the nanometer scale would lead to understanding functional responses in new nanomaterials and devices that could essentially impact a broad base of refrigeration technology [1-3]. Magnetic thin films are particularly promising for applications of a cooling device for Micro Electro Mechanical Systems (MEMS) and Nano Electro Mechanical Systems (NEMS) [1,2]. Their large surface area will also provide better heat exchange with the surrounding materials. While most work focused on bulk magnetocaloric materials, there is an increasing trend in magnetocaloric thin films research.

As compared to their bulk counterparts, smaller values of ΔSM are generally obtained in thin film materials [3]. Through a comparative MCE study on bulk, nanoparticle, and thin film samples of the same compound $La_{0.7}Ca_{0.3}MnO_3$, Lampen et al. have demonstrated that reducing the dimensionality of a ferromagnetic material tends to broaden and shift the TC to lower temperatures, while decreasing the MS and the magnitude of -ΔSM [4]. Recently, a novel approach, as proposed by Moya et al. [5], that exploited the structural phase transitions of $BaTiO_3$ to manipulate lattice strain of $La_{0.7}Ca_{0.3}MnO_3$ thin films has resulted in many

fascinating physical properties, including the new discovery of a giant reversible extrinsic magnetocaloric effect effect in the La0.7Ca0.3MnO3 film due to strain-mediated feedback from $BaTiO_3$ substrate near its first-order structural phase transition. It has been theoretically predicted that the confinement of spins in the direction perpendicular to the surfaces leads to a considerable enhancement of the MCE in Dy thin films [6]. The MCE study of ferromagnet/paramagnet multilayer structures using Landau phenomenological theory of phase transitions also demonstrates the possibility of achieving enhanced RC with such structures [7]. These important findings stimulate further MCE studies in thin film materials [6,7].

Since Gd is the benchmark refrigerant material for room temperature magnetic cooling application, numerous efforts have been made to explore the large MCEs and RCs in Gd based thin films [2,4]. In particular, a recent study has shown that the $Gd_5Si_{2.7}Ge_{1.3}$ thin film possesses a large MCE ($-\Delta SM \sim 8.83$ J/kg.K for $\Delta H = 5T$) and presents a broader magnetic response in comparison with its bulk counterpart [9]. While fabrication parameters/conditions are crucial in determining films quality and hence their MCE responses [8-9]. Although in principle, such films will be easier to integrate into electronic structures for application. However, with the currently available magnetic materials, this high efficiency is only realized in high magnetic field. Nano structuring is promising route to perturb properties, and may lead to novel and advantageous magnetocaloric properties usinf exinting materials.

To address these important issues, the Gd based alloys will be prepared by the sputtering technique in two different forms that are: thin films and heterostructures. In both cases, we will focus on:

- The effect of Co and Tb concentration on magnetic and magnetocaloric properties.
- The possibility of improving the relative cooling power, along with the operating temperature range as a micro-magnetic refrigerator.

To address the above mentioned objectives and to provide a comprehensive analysis of the magnetocaloric effects in Gd alloy-based thin films and heterostructures, the thesis is organized as follows:

Chapter 1 gives a brief review for the development of the domain of magnetic cooling, especially the efforts in near room-temperature refrigeration applications. An introduction of

the magnetocaloric effect and its thermodynamics is given in order to lay solid grounds for the other Chapters in this thesis. Theoretical models dealing with the universality of magnetocaloric effect and the relationships between the critical exponent and magnetocaloric effect are evaluated. Direct and indirect magnetocaloric effect measurements are described. An overview of magnetocaloric materials is presented.

Chapter 2 describes the working principles of the experimental technique used in this thesis. The sputtering technique for preparing Gd thin films and Gd alloy thin films. After each stage, the structural and magnetic properties of the samples can be characterized. The principals of primary characterization techniques are explained.

Chapter 3 regroups the most important results of the present thesis, and is divided into two major parts: (***i***) the first considers the Magnetic Properties and Magneto-Caloric Effect in $Gd_{100-x}Co_x$ Thin Films, while the second (***ii***) deals with Engineered Gd-Co based multilayer stack to enhanced magneto-caloric effect and relative cooling power.

Chapter 4, the structural, magnetic/magnetocaloric properties of Gd-Tb based alloys thin films are studied. In particular, multilayers [Gd/Tb] are investigated to study how magnetocaloric effect can be tuned using nanoscale material.

Finally, a **general conclusion** is drawn along with some perspectives.

Chapter 1:

Magnetocaloric refrigeration and material: state of the Art

1.1 Context

1.1.1 Age of the energy trilemma

We are entering the age of the Energy Trilemma [1]: not only do we need effective management of primary energy supply from domestic and external sources to ensure energy security and energy equity, but also, we face the challenge of achieving energy supply from renewable and other low-carbon sources. Energy consumption in residential and commercial buildings accounts for about 40% of total primary energy use in the European Union [2]. Cooling in its various forms (air conditioning, refrigeration, freezing, and chilling) takes up at least 15% of this figure [3]. Therefore, improving energy efficiency with respect to refrigeration plays an important role in reducing the overall energy consumption. Even marginal efforts in reducing power consumption in household and industrial refrigeration will have a large economic and ecological impact due to the size of this area. Today, nearly all commercial refrigeration and air-conditioning devices work with the gas compressor system (figure 1.1), which benefits from the energetic difference between gas and liquid to provide cooling via the expansion and contraction of a volatile refrigerant. Since their commercialization in the 1850s, hardly few other technologies have been able to compete on efficiency, price, or manufacturability.

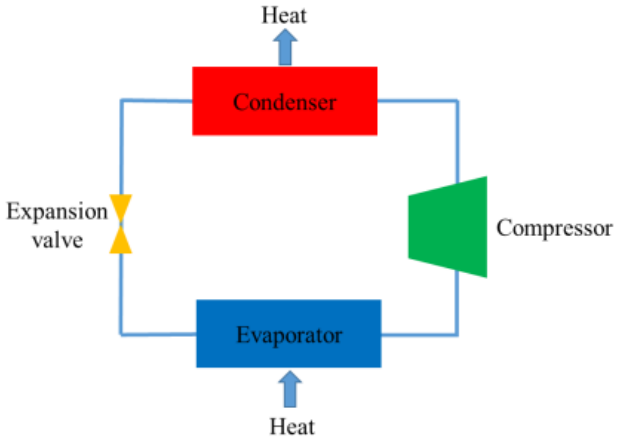

Figure 1. 1*: Simplified representation of the vapor compression cycle*

However, the vapor compression refrigeration poses serious threats to the environment. The refrigerant gases such as fluorocarbons have been phased out due to its ozone depletion potential. Most other volatile refrigerants in use today are also classified as greenhouse gases.

A 2009 study predicted that hydrofluorocarbons (HFCs) could account for between 28 and 45 percent (CO2-equivalent basis) of projected global CO2 emissions by 2050 [4]. Even though they are contained in refrigeration and air conditioning equipment during short-term application, there are long-term issues as to what to do with the buildup of HFC reservoir. Scientists today advocate earlier phase-outs of HFCs, which can provide as much as 40 percent more benefits for climate change because of reduction of the reservoir [5]. Vapor compression has been the leading technology for the last century after outcompeting natural ice as the primary source of refrigeration. Today vapor-compression is a reliable and low-cost technology; however, possible improvements are limited. What are alternative solutions that contribute to an overall reduction in the carbon footprint of cooling systems.

1.1.2 Alternative solution

Among others, a number of alternative refrigeration technologies exist today, including thermoacoustic [6], thermoelectric [7], and magnetic refrigeration. The concept of room temperature magnetic refrigeration can be understood as an analogue of the conventional gas compression and decompression system. Based on the magnetocaloric effect of suitable magnetic materials, this gas-free alternative solution harnesses the energy difference between different magnetic states in suitable solid refrigerant through magnetization and demagnetization cycles. When applied in household refrigerators, we expect a 25-30 percent efficiency improvement over vapor compression for this technology [8], which is equivalent to about 60% of Carnot efficiency [9]. This advantage in energy efficiency and environmental benefits make this technology particularly interesting for air-conditioning or domestic refrigeration applications.

Besides the efficiency improvement, a few other improvements can be expected from the magnetic refrigeration technology. A noise-reduction can be achieved due to few numbers of movable parts. Magnetic refrigeration can be used under ambient pressure with the heat transfer fluid. Since the high-pressure environment is no longer an issue, it is possible to use plastic casting that is less sophisticated and lightweight. In practice, the magnetic refrigerant changes states when moved in and out of the magnetic field of a permanent magnet. The principle of a magnetic refrigeration cycle is illustrated in figure 1.2. With the application and removal of the

field, the magnetocaloric material responds with a temperature change. A heat exchange fluid can then transfer the heat from or to the refrigerant at appropriate parts of a magnetic cooling cycle. Magnetocaloric technology can be used in both cooling application such as refrigeration and air conditioning and in heating applications like water heaters and clothes dryers.

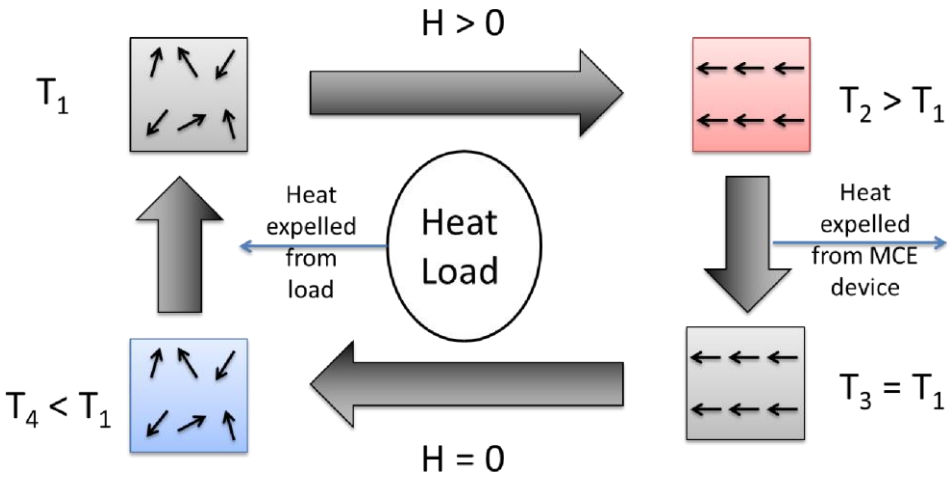

Figure 1. 2: *The four stages of a magnetic refrigeration cycle: (1) adiabatic magnetization, (2) remove heat, (3) adiabatic demagnetization, and (4) cool refrigerator contents.*

In addition, the reversal use of magnetocaloric effect can result in power generation. By taking advantage of the low value waste heat from various sources, magnetocaloric materials can be heated and cooled. Thermomagnetic generators can then convert the corresponding changing magnetization to electricity with a coil [10]. This application is a prospective recycling method for the waste heat generated in both urban setting and industrial environment.

1.2 General notions

Generally speaking, any thermal response of a material to an external applied field can be defined as a Caloric Effect. The different caloric effects can be classified based on the nature of the external stimulus, such as magnetic field (magnetocaloric effect), mechanical stress (elastocaloric effect), hydrostatic pressure (barocaloric effect), electric field (electrocaloric effect), and soon.

The core of magnetic refrigeration is the emission or absorption of heat in any suitable material in response to a changing magnetic field, i.e. the magnetocaloric effect (MCE). It is an intrinsic property of some magnetic materials. In a simplified definition, MCE is described as a reversible temperature change of a material as it undergoes a change in external magnetic field (magnetization and demagnetization) under adiabatic conditions. The conventional MCE occurs when the temperature increases upon application of a magnetic field, and the inverse MCE results in a decrease of temperature upon the application of a magnetic field.

1.2.1 From history to demonstration unit

In 1917 and 1918, French and Swiss physicists P. Weiss and A. Piccard first discovered a reversible heating of a Nickel sample near its Curie temperature (627 K) when a magnetic field was applied [11, 12]. A "novel magnetocaloric phenomenon", they called it. Historically, the discovery of the MCE was attributed to German physicist E. Warburg. This mis-citation has percolated through the literature for two decades. Recently, A. Smith reexamined the original works and found that the work of E. Warburg in 1881 [13] was the first to explain magnetic hysteresis but it was the work of Weiss and Piccard that should be acknowledged for the observation of the MCE [14].

Debye [15] and Giauque [16] independently suggested in the 1920s that this effect can be used to reach ultra-low temperature (<1 K). In 1933, Giauque and MacDougall first experimentally demonstrated how adiabatic demagnetization of paramagnetic salts like $Gd_2(SO_4)_3.8H_2O$ can be used to reach 0.25 K [17]. Adiabatic demagnetization was soon developed into a standard laboratory to reach millikelvin temperature, prior to the advent of dilution refrigerator, that is.

In the late 1970s, it has been recognized that a much larger MCE can be obtained in a ferromagnet in the vicinity of its Curie temperature and the effect can be used for heat pumping near room temperature [6]. G.V. Brown achieved a first breakthrough on magnetic refrigeration close to room temperature in 1976 with Gadolinium as the working material [18]. In his report, Brown showed that with an external applied magnetic field of 7 T, Gd produced an isothermal entropy change of 4 J/kg·K or an adiabatic temperature change of 14 K at its Curie point. Brown showed that a continuously operating device working near room temperature could achieve much larger temperature spans than the maximum observed MCE. After 50 cycles, a maximum

temperature span of 47 K was attained. The cyclic operation to maintain a large temperature span between the hot and cold sources is where magnetic refrigeration differs from adiabatic demagnetization. This prompted the development of various devices and led to the establishment of the Active Magnetic Regenerator (AMR) cycle, described by J. A. Barclay in 1983 [19]. By virtue of accumulating temperature span with fluid cycles, AMR allows improved exploitation of the magnetocaloric effect, giving rise to the consideration of magnetic refrigeration as a potentially viable technology.

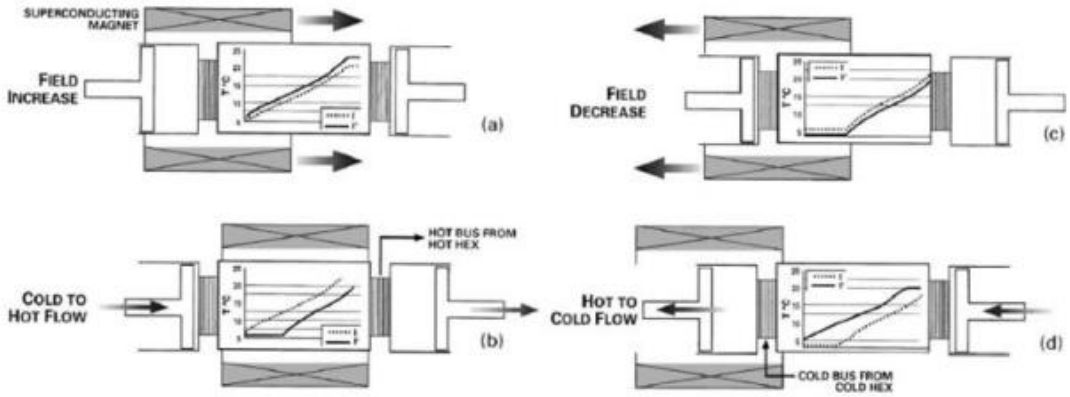

Figure 1. 3*: The principles steps in a refrigeration cycle using active magnetic regenerator (AMR), taken from reference [20].*

The principle steps are shown in figure 1.3. In this system, the magnetocaloric material is used as both a thermal regenerator, which stores temporarily the positive or negative temperature variation and then exchange with the heat transfer fluid, and the active magnetic component that induces the temperature change. Regeneration allows the heat rejected by the system at a step of the cycle, to be restored and given back to the system at another step of the cycle. It is considered that the refrigerant material has a flat initial temperature profile between cold and hot sources. The four steps of this cycle are the following:

a) Adiabatic magnetization: the whole regenerator temperature increases.

b) Isofield cooling: the calorific fluid flows from the cold source toward the hot source thus evacuating heat and creating a thermal gradient in the regenerator.

c) Adiabatic demagnetization: the whole regenerator temperature decreases.

d) Isofield heating: at zero field, the fluid flows from the hot source towards the cold source, thus gives its heat to the hot side of the refrigerant and increases the thermal gradient.

In such an AMR cycle, the geometry of the regenerator will determine the efficiency of the heat transfer. This is the reason why we normally find the magnetocaloric material used in the shape of a porous bed or a superimposition of plates spaced to facilitate fluid exchange.

As the refrigerant material also acts as a regenerator, the temperature span of an AMR cycle can widely exceed the temperature variation of the material. Moreover, the regenerator can have several layers of magnetocaloric material or composite materials in order to extend the working temperature range and bring about higher performance of the system. In an example of a domestic refrigerator, the cold source is typically less than 269 K and the hot source around the ambient temperature is expected to be around 293 K in average.

In 1997, Pecharsky and Gschneider showed a "giant" MCE in Gd5Si2Ge2, setting a milestone in magnetocaloric effect for potential room-temperature cooling application [21]. The MCE of Gd5Si2Ge2 was about 50% larger than that of Gd metal, and the authors attributed this to a coupled first-order magneto-structural transformation.

Based on this result, Zimm and colleagues designed the first proof-of-principle near room temperature magnetic refrigerator unit (Figure I-4) in 1998 [22]. Using commercial grade Gadolinium metal, this demonstration unit was capable of delivering a maximum cooling power of 600 watt and ran for over 5000 hours during an 18-month period with no significant problems and only minor maintenance.

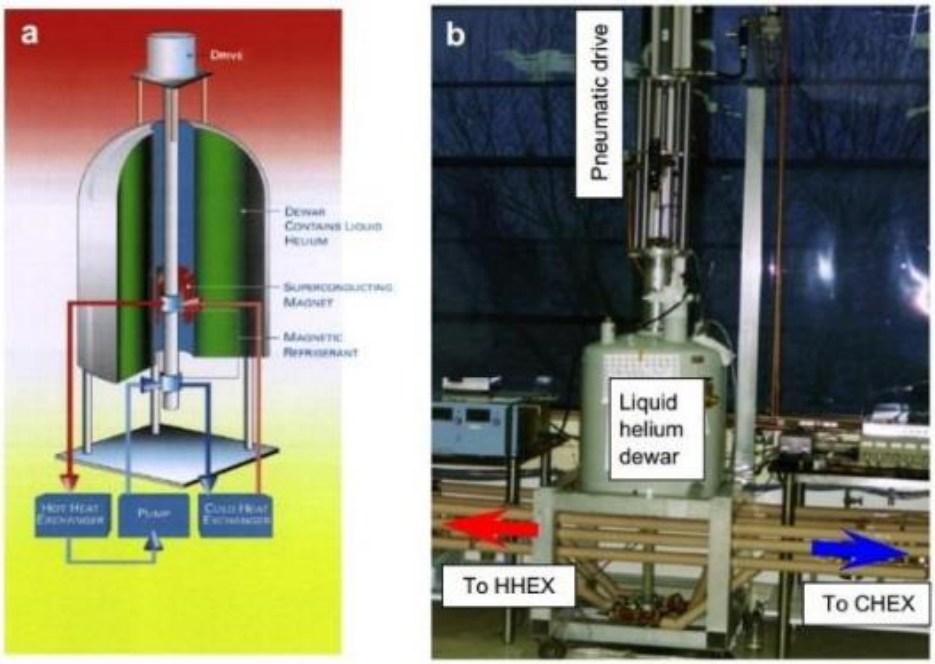

Figure 1. 4*: (a) Schematic and (b) photograph of the Ames Laboratory/Astronautics Corporation of America's reciprocating proof-of-principle magnetic refrigerator, taken from [22].*

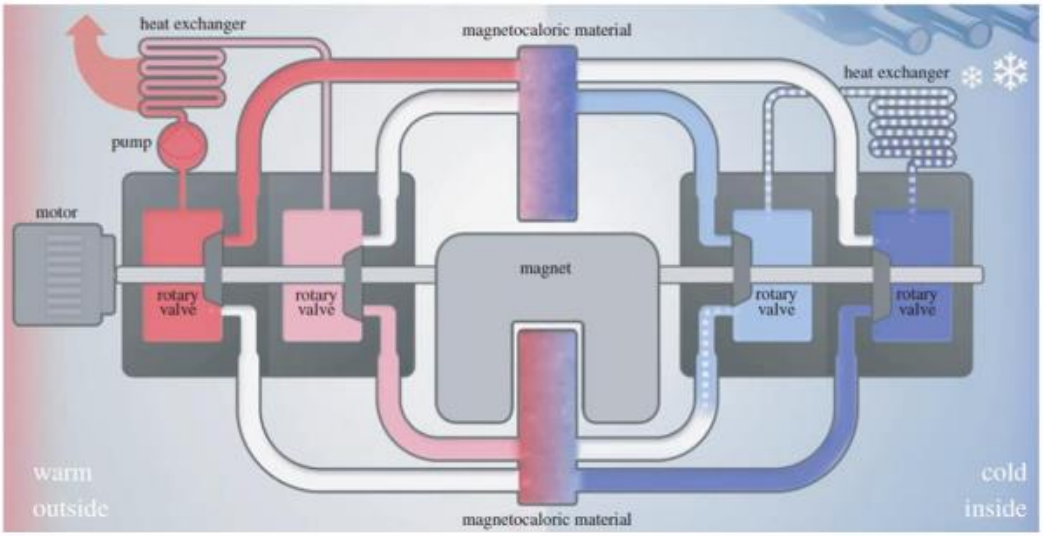

Figure 1. 5 *: Schematic picture of a magnetocaloric wine cooler using MnFePSi type of materials, taken from reference [24].*

These events stimulated a new wave of research on both the materials front and the device design department. In 2015, Haier, Astronautics Corporation of America, and BASF presented the first industrial proof-of-concept wine cooler based on a magnetocaloric heat pump at the International Consumer Electronics Show (CES, Kan.6-9, 2015) in Las Vegas, USA [23]. The basic working principle of the prototype wine cooler using magnetocaloric material is shown in figure 1.5.

Although the magnetic cooling technology has not been yet commercialized at the time of writing, currently a few companies are involved in the manufacturing of magnetic refrigeration technology, including (in alphabetical order) Astronautics Corporation of America (U.S.), BASF SE (Germany), Camfridge Ltd (U.K.), Cooltech Applications (France), ERAMET SA (France), General Electric CO. (U.S.), Hitachi metals (Japan), Qingdao Haier Co., Ltd (China), Vacuumschmelze GmbH & Co. KG (Germany), Samsung Electronics Co., Ltd (South Korea), Sigma-Aldrich Corporation (U.S.), Toshiba Corporation (Japan) and Whirlpool Corporation (U.S.). Many challenges still lie ahead to achieve a commercial magnetic refrigeration system at room temperature, among which a great deal of the physics is still yet to be understood completely. In the next section, some basic notions and theories related to magnetocaloric phenomenon will be presented.

1.2.2 Magnetocaloric Effect (MCE): thermodynamic principals

Theoretical description of the MCE will help us build fundamental frames in which the common notions in magnetocaloric materials shall be introduced. This reversible (heating or cooling) effect can be generally represented by the **adiabatic temperature change** (ΔT_{ad}) or the **isothermal entropy change** (ΔS_M). The principal subject in the following section is what is classified as conventional MCE, which means that the material heats up upon magnetization (negative ΔS_M) and cools down upon demagnetization (positive ΔS_M). Within the conventional MCE systems, paramagnetic materials are out of the scope of this work, as they exhibit very small relative entropy change except at very low temperatures. Room temperature magnetic refrigeration generally involves ferromagnets, which are the most frequently studied systems to illustrate magnetocaloric effect.

In order to describe the thermodynamic potential of a magnetic material under a magnetic field, we use the description of the Gibbs free energy, G, as a function of the internal energy, U, intrinsic variables such as volume, V, entropy, S, and magnetization, M (the magnetic dipole moment per unit volume), and extrinsic parameters such as temperature, T, pressure, P, and applied magnetic field, H (μ_0 denotes the vacuum permeability).

$$G = U + PV - M.\mu_0 \mathrm{H} - TS \tag{1.1}$$

The differential free energy of the system as a function of the state functions T, P, is given by

$$dG(T, \mathrm{H}, P) = (\frac{\partial G}{\partial T})_{H,P} dT + (\frac{\partial G}{\partial H})_{T,P} dH + (\frac{\partial G}{\partial P})_{T,\mathrm{H}} dP \tag{1.2}$$

The total differential can be written as

$$dG(T, P, \mathrm{H}) = dU + VdP + PdV - \mu_0 MdH - \mu_0 HdM - TdS - SdT \tag{1.3}$$

Recall the first law of thermodynamics: $dU\,(T, P, H) = TdS + \mu_0 HdM - PdV$, we can simplify Eq.(I-2) to the following equation

$$dG(P, H, T) = VdP - \mu_0 MdH - SdT \tag{1.4}$$

From Eq. (I.4) and analogy to Eq. (1.2), we can derive the expression for both the entropy and the magnetization of the system:

$$S(T, P, H) = -\left(\frac{\partial G}{\partial T}\right)_{H,P} \tag{1.5}$$

$$\mu_0 M(T, P, H) = -\left(\frac{\partial G}{\partial H}\right)_{T,P} \tag{1.6}$$

With Eq. (1.5) and (1.6), the well-known Maxwell relation can be obtained,

$$\left(\frac{\partial S}{\partial H}\right)_{T,P} = \mu_0 \left(\frac{\partial M}{\partial T}\right)_{H,P} \tag{1.7}$$

Under constant temperature and pressure, we can derive the entropy differential as

$$dS = \mu_0 \left(\frac{\partial M}{\partial T}\right)_{H,P} dH \tag{1.8}$$

The isothermal entropy change from the change in external magnetic field can then be obtained through integrating Eq. (1.8),

$$\Delta S_M(T,P,\Delta H) = S\left(T,P,H_f\right) - S(T,P,H_i) = \mu_0 \int_{H_i}^{H_f} \left(\frac{\partial M}{\partial T}\right)_{H,P} dH \quad (1.9)$$

The entropy change induced by external field is generally calculated from magnetization data. On the other hand, the entropy change can be expressed in terms of specific heat under constant pressure, $C_p(T,H) = T\left(\frac{\partial S}{\partial H}\right)_H$, according to the second law of thermodynamics [25]:

$$\left(\frac{\partial S}{\partial T}\right)_H = \frac{C_p(T,H)}{T} \quad (1.10)$$

which allows us to calculate the isothermal entropy change from the heat capacity:

$$\Delta S_M(T,\Delta H) = \int_0^T \left(\frac{C_p\left(T,H_f\right) - C_p(T,H_i)}{\partial T}\right) \quad dT \quad (1.11)$$

Another important parameter used for the characterization of magnetocaloric materials is the **adiabatic temperature change.** The temperature change in a material during adiabatic magnetization under isobaric conditions is

$$\Delta T_{ad} = T_{f,Hf} - T_{i,Hi} \quad (1.12)$$

where H_f and H_i represent the final and initial applied magnetic field ($H_i < H_f$). In order to associate temperature with entropy, let us consider the total differential of the entropy:

$$dS\ (P,T,H) = (\frac{\partial S}{\partial P})_{T,H} dP + (\frac{\partial S}{\partial T})_{P,H} dT + \mu_0 (\frac{\partial S}{\partial H})_{P,T} dH \quad (1.13)$$

Under adiabatic and isobaric conditions, the following assumptions can be written:

$$(\frac{\partial S}{\partial P})_{T,H} dP = 0 \quad (1.14)$$

$$dS = 0 \quad (1.15)$$

Eq. (1.13) can now be rewritten as

$$dT = -\mu_0 (\frac{\partial S}{\partial H})_T (\frac{\partial T}{\partial S})_H dH \quad (1.16)$$

By taking into account the Maxwell relation and the definition of the specific heat under constant pressure previously mentioned, the right hand side of Eq. (1.16) can be replaced by a specific heat term and a magnetization term and we obtain

$$dT = -\mu_0 \frac{T}{C_p(T,H)} \left(\frac{\partial M}{\partial T}\right)_H dH \tag{1.17}$$

Although the right hand side of Eq. (1.17) is not an exact differential, we can "integrate" to get the expression of the adiabatic temperature change ΔT_{ad}.

$$\Delta T_{ad}(T, \Delta H) = -\mu_0 \int_{Hi}^{Hf} \left(\frac{T}{C_p(T,H)}\right)_H \left(\frac{\partial M(T,H)}{\partial T}\right)_H dH \tag{1.18}$$

It is important to note that the integral is not independent of the integration path so this relation has to be evaluated explicitly along the relevant isentrope (constant entropy line). Both magnetization and heat capacity are required to determine ΔT_{ad}, a so-called indirect technique.

Figure 1.6 illustrates the effect of an external field changing from changing from H_i to H_f on the entropy and spin system of a ferromagnetic material. The material undergoes a ferromagnetic to paramagnetic transition upon cooling. Different path lines are used to show the relation between ΔS_M and ΔT_{ad} in such transition.

Path A→B corresponds to the process of increasing magnetic field while keeping temperature constant, i.e. the isothermal magnetization process. The ordering of the system results in a decrease in the magnetic part of the entropy, ΔS_M. In an adiabatic environment, no heat exchange takes place between magnetic solid an its surrounding.

Along path B→C, adiabatic demagnetization takes place. The field change occurs while the entropy stays constant, $\Delta S_M = 0$. The resulting temperature difference,

$\Delta T_{ad}, is\ then\ the$ "cooling" effect associated with the removal of he external field in conventional MCE. The described temperature change is the manifestation of the MCE.

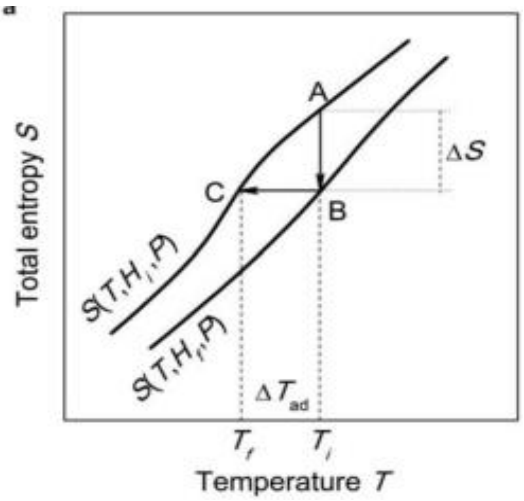

Figure 1. 6*:* Schematic representation of the effect of an external field changing from H_i to H_f ($H_i < H_f$) on the entropy of a magnetic material, illustrating the relation between ΔS_M and ΔT_{ad} adapted from reference [26]

1.2.4 Order of transition and critical phenomena

In second order magnetic transition (SOMT) materials, the nature of a paramagnetic to ferromagnetic (PM-FM) transition and magnetic interactions around this transition are quantitatively determined by a set of critical exponents [27-29], which have recently been correlated with the MCE behaviors of the materials [30]. Based on the scaling hypothesis, the critical behavior of a SOMT system can be characterized by the critical exponents of β, γ, and δ, which are associated with the spontaneous magnetization MS(T), inversely initial susceptibilityχ_0^{-1} (T), and critical isotherm M at T_C, respectively [31]. These exponents can be defined by the following power-law relations:

$$M_s(T) = M_0(-\varepsilon)^{\beta} \tag{1.19}$$

$$H = DM^{\delta} \tag{1.20}$$

$$\chi_0^{-1} = (\frac{H_0}{M_0})\varepsilon^{\gamma} \tag{1.21}$$

where ε is the reduced temperature $\varepsilon = (\frac{T-T_C}{T_C})$; M_0, H_0 and D are the critical amplitudes.

These three critical exponents are in the Widom scaling relation $\delta = 1 + \frac{\gamma}{\beta}$ [32]. From the isothermal magnetization curves near T_C, the critical exponents can be accurately obtained by the Kouvel-Fisher (K-F) method [33]. The brief description of this technique is as follows: Firstly, the modified

Arrott plots ($M^{1/\beta}$ vs. $(H/M)^{1/\gamma}$) can be drawn with chosen initial values of β and γ, based on the Arrott-Noakes equation of state given by $(\frac{H}{M})^{\frac{1}{\gamma}} = \frac{T-T_C}{T_1} + (\frac{M}{M_1})^{\frac{1}{\beta}}$ [34].

Then, by linearly extrapolating the high field region of the plots, the intercepts of the $M^{1/\beta}$ axis will generate a new series of $M_S(T)$ values, similarly $\chi_0^{-1}(T)$ can be obtained by the intersections of the $(H/M)^{1/\gamma}$. The following linear relations can be easily derived from Eq. (1.19) and (1.21).

$$M_s(T)[\frac{dM_s(T)}{dT}]^{-1} = \frac{T-T_C}{\beta}, \tag{1.22}$$

$$\chi_0^{-1}(T)[\frac{d\chi_0^{-1}(T)}{dT}]^{-1} = \frac{T-T_C}{\gamma} \tag{1.23}$$

Hence, new values of β and γ can be determined from the slopes of the linear fitting. Afterwards, the new values of β and γ are reintroduced into the new $M^{1/\beta}$ vs. $(H/M)^{1/\gamma}$ plots to repeat the first step. The optimal values of critical exponents can be thusly obtained by this iteration converge process. To check reliability of the obtained exponents, two unambiguous-universal curves for $T > T_C$ and $T < T_C$ are often constructed from the log-log scale plots, which satisfy the scaling hypothesis described by $|\varepsilon|^{-\beta} = f_{\mp}\left(H\varepsilon|^{-(\beta+\gamma)}\right)$, , where f_+ for $T > T_C$ and f_- for $T < T_C$ are regular analytical functions. From the scaling equation of state in the form of $\frac{H}{M^{\delta}} = h(\frac{\varepsilon}{\frac{1}{M^{\beta}}})$, where $h(x)$ is the scaling function, the plot of $\frac{H}{M^{1/\delta}} vs \frac{\varepsilon}{\frac{1}{M^{\beta+\gamma}}}$ should also collapse into a universal curve.

1.2.5 Universal scaling

In addition to characterizing the practicality of a magnetic refrigerant, the magnetic field and temperature dependence of ΔS_M can also be exploited as a fundamental tool for probing the

nature of magnetic transitions and magnetic ground states in complex magnetic systems [35-37]. This method has been based on evaluation of changes in sign and magnitude of $(\partial M/\partial T)_H$ and hence $\Delta S_M(T,\mu_0 H)$ with respect to the nature of magnetic phase transitions (FOMT or SOMT, or both) that are present in the material [35]. It has been shown that a magnetic material undergoing a paramagnetic to ferromagnetic transition will exhibit $\Delta S_M < 0$ and $\Delta T_{ad} > 0$ (the "*conventional*" magnetocaloric effect), since the entropy in the ferromagnetic region decreases as the increasing strength of $\mu_0 H$ suppresses thermal fluctuations in the magnetic sublattice [38-40]. On the other hand, an *inverse* magnetocaloric effect ($\Delta S_M > 0$ and $\Delta T_{ad} < 0$) is observed near ferromagnetic to antiferromagnetic transitions as the application of a magnetic field to noncollinear magnetic structures can decouple spins from the sublattice aligned in opposition to the applied field direction, introducing disorder into the total spin system and increasing the magnetic entropy [41-43]. Figure 1.7 shows an example of the conventional and inverse magnetocaloric effects that have been observed in the same material $Pr_{0.5}Sr_{0.5}MnO_3$ [42].

In case of a conventional ferromagnetic material exhibiting the conventional MCE, the peak entropy change at the Curie temperature (T_C) increases with magnetic field according to $\Delta S_M^{max} \sim H^n$ where $n = 2/3$ for the mean field case, but can vary according to the nature of the magnetic interactions in the system [38]. For a family of $\Delta S_M\ (T)$ curves acquired under different magnetic fields, the scaling hypothesis that governs materials undergoing a second-order magnetic transition predicts that the points at a particular fractional value with respect to the peak entropy change (e.g. $\Delta S_M = 0.5 * \Delta S_M^{max}$) are in an equivalent magnetic state for each of the iso-field curves. Therefore, appropriate re-scaling of the entropy and temperature variables based on these equivalent points then leads to the collapse of the $\Delta S_M\ (T.H)$ curves onto a single universal curve, the so-called "universal curve" method as proposed for the first time by Franco *et al.* [44] and being employed widely in literature for accessing the MCE behaviors of magnetic materials [38]. The universal master curve of $\Delta S_M\ (T.H)$ can be obtained by collapsing all ΔS_M *vs.* T curves at their external fields through $-\Delta S_M$ normalized to $-\Delta S_M^{max}$. Their temperature axes also need to be rescaled by equation [38,44]:

$$\theta = \begin{cases} -(T - T_C)/(T_{r1} - T_C) & T \le T_C \\ (T - T_C)/(T_{r2} - T_C) & T \ge T_C \end{cases} \quad (1.8)$$

where T_{r1} and T_{r2} are two reference temperatures above and below T_C which should be satisfied the relation

$$-\Delta S_M^{max}(T_{r1}) = -\Delta S_M^{max}(T_{r2}) = f \times (-\Delta S_M^{max}) \qquad (1.9)$$

f is often chosen to be 0.5. It has been shown that if the re-scaled $\Delta S_M(T)$ curves of a magnetic refrigerant collapse onto one universal curve then the magnetic transition of the material is said to be of second order [38,44]. If the curves fail to collapse into one curve then the underlying assumptions of the scaling hypothesis breaks down, which is a property of FOMTs [45] or of multiphase systems [46].

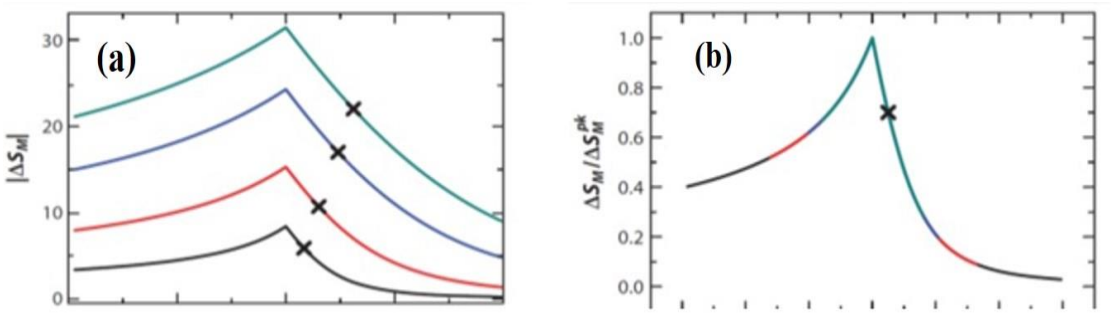

Figure 1. 7:A phenomenological construction of the universal curve: (a) identification of the reference temperatures and (b) rescaling the temperature axis to place T_r at $\theta = 1$. Adapted from Ref. [4].

1.3 Magnetocaloric materials

The magnetocaloric effect is present in all materials but is significant in magnitude near magnetic phase transitions. Most work has focused on materials containing rare earth elements, since the entropy change scales with magnetic moment per atom. With supply chain and related price stability issues, there have also been relatively new efforts to explore magnetocaloric materials that do not contain rare earth elements, including transition metal glasses [47]. The advantage of transition metal systems may in fact be in Joules-per-stable-dollar rather than Joules-per-kilogram [48].

As noted by Sandeman [49] it is quite feasible that many advances in magnetic refrigeration may be realized simply by "intelligent synthesis" using existing materials. Philosophically, using the tools of nanoscience allows us to exploit structure–property relationships to appropriately tailor known materials for magnetocaloric applications. This approach is thus essentially a way to broaden the search for magnetocaloric materials that complements the parallel search for brand new systems. Historically, Morelli et al. appear to have published the first thorough film-based MCE study [50] Though with 2.4 μm thickness their lanthanum manganite films were essentially bulk, that work demonstrated thin film techniques led to high quality films with quite reasonable MCE behavior.

Thus far, some ubiquitous responses emanate from surveying studies in this area. First, entropy change peaks for nanoscale films show reduced maximum entropy change and enhanced temperature breadth, relative to bulk. This is shown for Gd in figure 1.8 for a field change of 10 kOe, in which one observes drastically different entropy change response in as-grown films relative to the bulk: a reduction of the temperature at which the entropy change is maximal (T_{peak}) from 292 K to 265 K, and a near doubling of the full width at half max from 34 K to 65 K. The origin seems to be a combination of finite size effects and defects. Second, well controlled fabrication of heterostructures leads to turnabilities related to interfacial effects and atomic order. Third, strain is emerging as a significant tool, leading to variable properties in second order materials, suppressing the irreversibility of first order magneto-structural transitions, and allowing phase transitions to be triggered extrinsically.

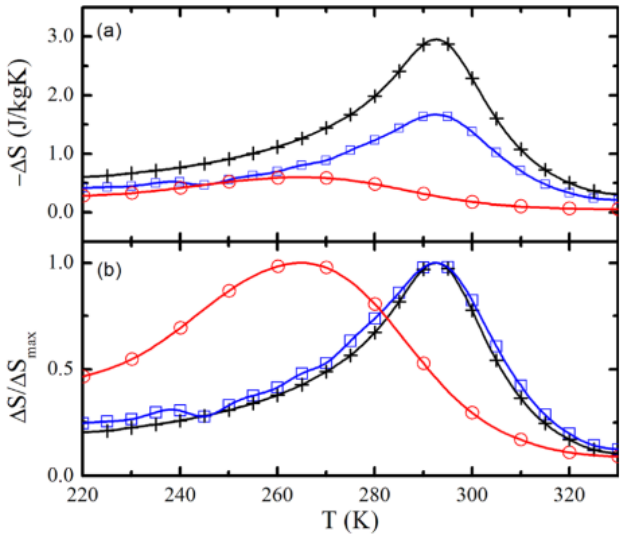

Figure 1. 8: (Color online) (a) ΔS(ΔH, T) for a 300 A˚ thick Gd film grown at RT (red circles), a 300 A˚ thick Gd film grown at 450 C after a gettering process (blue squares), and bulk Gd (black crosses). The ΔS_{max} were 0.60, 1.7, and 2.9 J/kg K, respectively, for ΔH =10 kOe. (b) Same data normalized by ΔS_{max} [93].

1.3.1 Finite size effects:

Theoretical investigations suggest that geometrical confinement of Dy and Ho can lead to enhanced magnetocaloric effect relative to the bulk [51,52] The truncated lattice implies the spins near the surface experience reduced exchange from second nearest-neighbors. This causes ferromagnetic ordering to become energetically favored near the surface, relative to helical ordering. Simultaneously, the surface spins are more compliant to the external field, allowing the Zeeman energy to play a more significant role in the material's magnetic response (similar effects have been reported in nanoparticles [53]). Ultimately, the helical magnetic state loses favor to a stable ferromagnetic arrangement of spins if the film thickness is near or below the helical period (e.g., 5–10 atomic layers). While not yet realized in experiment, the prediction of greater MCE in thin films over the bulk is intriguing.

Jiang et al. reported significant MCE in epitaxial CrO_2 films grown on TiO_2 by chemical vapor deposition [54] The transition temperature for CrO_2 is around 385 K, and the associated entropy peak magnitude was 8.5 J/kg K for a 50 kOe field change. As with other films, the entropy peak occurs over an extended temperature range, leading to an inferred relative cooling power of 410 J/kg, rivaling that of bulk Gd.

1.3.2 Interface engineering:

In a very thorough study, Mukherjee et al. combined theory and experiment to show the tunability that can be realized for magnetocaloric via nanostructuring [55] That work focused specifically on Co/Cr superlattices designed to tailor metamagnetic transitions, leading to both positive and negative MCE. They showed that both interlayer and intralayer exchange interactions are important, and that systems designed with large ratios of the latter to the former can have large magnetic entropy changes.

Generally speaking, manganites ($R_{1-x}M_xMnO_3$) are rich in physics, with electronic and magnetic properties widely tunable by perturbations of the mixed valence of the Mn ions through chemical substitutions; quarternary and pentenary compounds are thus common. They are thus are among the most heavily studied materials for magnetocaloric effects [56,57] and thin film studies are following suit. Manganites lend themselves to heterostructuring dissimilar materials with atomically sharp interfaces. This fact was used by Zhang et al. [58] and Belyea et al. [59] to study the magnetocaloric properties in superlattices using $LaSrMnO_3$ (LSMO). Zhang studied $SrTiO_3/[LSMO_3(20)/SrRuO_3(1,3,6)]_{15}/LSMO3(20)$, wherein the parentheticals indicate the layer thicknesses in unit cells. They interestingly showed an enhanced moment mediated by the Mn and Ru charge states at the interfaces, leading to entropy change magnitudes similar to bulk LSMO. They also observed the typical broadened phase transition, leading to relative cooling powers exceeding that of polycrystalline LSMO. It is particularly noteworthy that these improvements were greatest when the SRO was 1 or 3 unit cells thick; the moment was reduced by 6 unit cells. The obvious next step here is to increase the density of these single unit cell interrupts.

Belyea et al. studied the impact of nanostructuring through "digital" synthesis relative to a random alloy. The films were epitaxial samples grown by ozone-assisted oxide molecular beam epitaxy [59]. The alloy was grown using codeposition in order to have randomly distributed La and Sr cations on the A-sites of the ABO_3 perovskite structure. Digital synthesis, in which the La and Sr are alternatingly deposited at subunit cell levels, leads to a superlattice of $LaMnO_3$ (LMO) and $SrMnO_3$ (SMO), with each layer having exclusively La or Sr, and each layer thus being a single unit cell of the perovskite structure. The superlattice structure had a net composition equivalent to that of the random alloy film. The maximum magnetic entropy change and relative cooling power of the alloy film exceeded those of the superlattice. The unique comparison in this study of an epitaxial alloy with random versus ordered A-site occupation leads to the conclusion that the cation disorder plays a role in the magnetocaloric effect in manganite materials.

1.3.3 Strain effects:

Strain can play a major role in thin films. The material is necessarily coupled to a substrate, and that interfacial coupling can change the physical properties of the film. The simplest example is the static lattice mismatch between film and substrate. Kumar et al., for example, showed that the magnetocaloric effect in LSMO thin films is dramatically different when grown on $LaAlO_3$, $SrTiO_3$, and $La_{0.3}Sr_{0.7}Al_{0.65}Ta_{0.35}O_9$ [60], and Maat et al. showed different transition temperatures in FeRh grown on MgO (001) and c-axis sapphire [61]. More complex examples may lead to interesting devices that extrinsically manipulate the magnetic material by altering the state of the substrate [62], or altering the material itself, e.g., through voltage control in multiferroic materials [63]. The latter, illustrated in Figure 1.9, is particularly exciting since it offers the prospect of magnetic cooling without the need for externally applied magnetic fields.

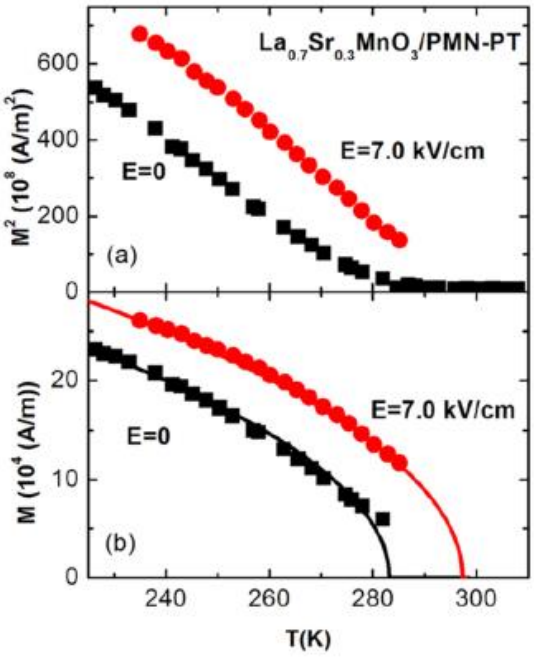

figure 1. 9 : Demonstration of voltage-controlled magnetization, and thus magnetic entropy available for magnetocaloric effects with applied electric fields of zero (squares) and 7.0 kV/cm (circles). (a) M_2 vs T representation of magnetization data of a LSMO (20 nm)/$Pb(Mg_{1/3}Nb_{2/3})O3$-$PbTiO_3$ (PMN-PT) [66]. (b) M vs T together with best fits of the Landau-type functional form of the magnetization (lines).

Recent work in the $La_{0.7}Ca_{0.3}MnO_3$ (LCMO) system highlights the impact of nanostructuring [64] Films exhibited enhanced refrigerant capacity relative to bulk polycrystalline material, despite the ubiquitous suppression of ordering temperature. Intriguingly, the first order magnetic phase transition in bulk LCMO appears to have been converted to second order (or at least converted to a continuous transition) in the film by the nontrivial film-substrate coupling. This is of interest with respect to reducing losses related to the hysteretic behavior of first order transitions.

The unique martensitic transformation in ferromagnetic shape memory alloys has given these materials myriad potential applications, including magnetocaloric effect [67-69]. These transitions typically involve strong magnetoelastic coupling, and are of first order. The unfortunate trade off with first order transitions is thermal hysteresis that can impact the

ultimate cooling power in a refrigeration cycle, and the potential misinterpretation of the underlying magnetic entropy change through inappropriate usage of the Maxwell relation. As noted by de Oliveira and von Ranke [70], determining the magnetic entropy change associated with first order transitions requires some care. In many cases, the data density required is significantly greater than typically used, and significantly greater than that required for second order transitions. One advantage of growing these materials in thin film form is the potential for reducing the first-order nature of the transition because of strong coupling to the substrate. In epitaxial NiCoMnIn films, for example, Niemann et al. found the portion of the film immediately coupled to the substrate remained in the ferromagnetic austenite phase, indicating that the coupling completely suppresses the martensitic transformation [71].Zhang et al.[72] showed the advantage of tailoring the thin film composition so that the magnetostructural martensitic transformation and the ferromagnetic ordering of the austenitic phase occurred simultaneously. NiMnGa films [73],while reduced from bulk material, still show appreciable entropy change of 8.5 J/kg K for a 60 kOe field change.

MnAs exhibits a first order magnetostructural phase transition between the low temperature hexagonal a-MnAs ferromagnetic phase and the high temperature paramagnetic orthorhombic b-MnAs phase. While there has been some work focused on tuning the phase transition by substitutions [74,75], strain engineering—a beautiful analog to the hydrostatic pressure sensitivity of bulk MnAs [76]in films is unlocking great potential. Mosca et al. [77] used strain to tune the MCE in 70 nm thick MnAs grown epitaxially on GaAs substrates by molecular beam epitaxy (Figure 1.10). While the transition appeared to remain first order, the range of temperatures allowing coexistence of the two constituent phases was extended, with the dominant transition temperature being increased relative to the bulk. Solzi et al. used metal–organic vapor phase epitaxy to grow MnAs on GaAs and oxidized silicon substrates. In contrast to Mosca et al., they found the first order transition on GaAs was essentially transformed to second order because of the strong coupling of the epitaxial 18 nm thick films to the substrate. When grown on oxidized silicon, the MnAs was polycrystalline and showed first order behavior presumably because it rapidly relaxed to its preferred structure. As a testament to the possibilities related to strain engineering, it was recently shown that acoustic

stresses can be exploited to drive the phase transition [78] in MnAs films with surface acoustic waves. This will certainly lead to neat devices that combine magnetocaloric and piezoelectric phenomena.

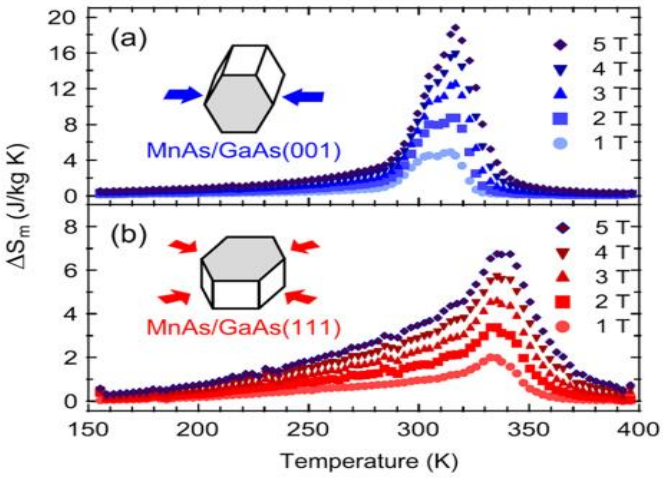

Figure 1. 10*:* Strain engineering can significantly impact both the peak position and amplitude of the magnetocaloric effect, especially in first order transitions [77]. Magnetic-entropy changes as a function of temperature and field for (a) MnAs/GaAs(001) and (b) MnAs/GaAs(111) epilayers. The magnetic field was applied parallel to the easy magnetic axis of the MnAs epilayers.

Chapter 2:

Experimental tools and samples

2.1 Introduction

From the elaboration of the first sample to the publication of the obtained results many instruments are necessary. The aim of this part is to describe the instruments I used during my thesis and the physical principals involved. First, we will focus on the techniques involved to obtain the samples. Then we will take a bit of time to describe the pieces of equipment involved in the magnetic characterization of the samples.

2.2 Fabrication of Gd Alloy Films and Heterostructures

2.2.1 Sputtering technique

In order to obtain magnetic thin films, several techniques are available, as for instance molecular beam epitaxy (MBE) or pulsed laser deposition (PLD). In this manuscript, all the samples have been elaborated in a magnetron sputtering tool. A magnetron sputtering tool is an enhanced type of sputtering tool. The principle of sputtering can be understood with figure 2.1.

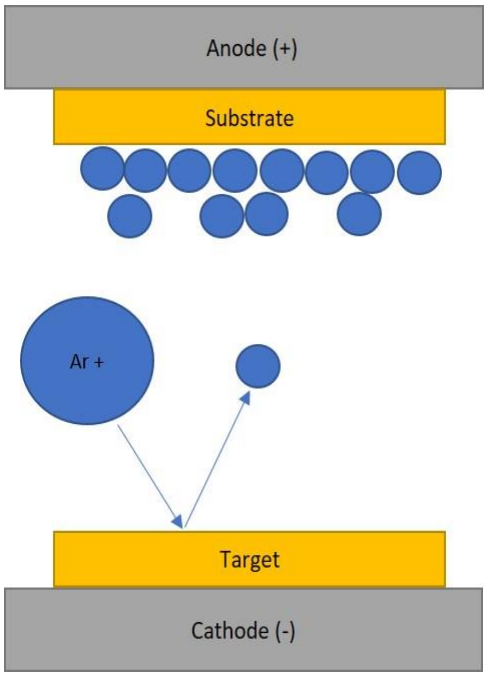

Figure 2. 1*:* Schematic of a sputtering system

In an ultra-high vacuum chamber (at a pressure around 5.10^{-8} Torr), argons atoms are injected. Then, a high voltage (of the order of hundreds of volts) is applied between the cathode (-) and the anode (+). As an effect, Ar atoms are ionized into Ar^+. Ar^+ ions are then electrically attracted by the cathode and hit the target because it is placed above the cathode. The target is composed of pure element that we want to have in our final sample, for instance Cu. Then, due to the collision between Ar^+ ions and the (Cu) target, (Cu) atoms are ejected from the target. Their trajectory is, in our case, mostly ballistic given that they have no specific electric charge. Since target atoms are ejected in every direction in the chamber, only a small part of the atoms reaches the substrate placed on top of the chamber. Those atoms together form the deposited layer. One parameter that is critical to achieve sputtering is the number of Ar+ ions. The number of Ar atoms initially present is not a limiting factor because Ar atoms are constantly injected into the chamber, but their ionization is not granted. The main mechanism of ionization of Ar atoms is through collision with electrons. An electron colliding with an Ar atom can eject another electron from the Ar atom (ionization of the Ar atom) and at its turn, the newly ejected electron can collide with another Ar atom. The initial ionization of Ar atoms can then create a cascade phenomenon and, if the ionization rate is high enough, the Ar+ plasma can be self-sustainable. In order to keep this ionization rate stable over time, a magnetron magnetic field is present at the surface of the target. Its role is to confine electrons, both from the Ar+ plasma and the target, due to the Lorentz force in the vicinity of the target. Magnetron sputtering can be used to grow layers composed of a single element or can be used to frm alloys. There are two possibilities in that case; either the sputtered target is already an alloy (this is the case IrMn), or the different species come from different target (as it is the case for GdTb or GdCo). For the deposition of insulating materials, we use a RF current to prevent the accumulation of charges on the surface of the target. One can note that it is possible to use a pulsed DC current to sputter insulating targets but we did note use it

2.2.2 Magnetron Sputtering

Among the different ways to enhance the sputtering process, the magnetron sputtering was the one chosen for most of the thin films deposition achieved during this thesis. The main difference between this one and a basic DC sputtering system described above is the addition

of a specific magnetic field configuration near the target area. In order to increase the ion density in the vicinity of the target, the system is equipped with two permanent magnets of opposite polarity located below the target (see figure 2.2). They create a magnetic field B parallel to the target surface and orthogonal to the electric field E used to ionize the argon. The combination of these two fields gives rise to field lines that trap the secondary electrons. The Lorentz force induced causes a helical movement of the electrons. The advantage of this is that the plasma is confined to an area near the target, without causing damages to the thin film being formed. Also, electrons travel for a longer distance, increasing the probability of further ionizing Argon atoms. This tends to generate a stable plasma with high density of ions. More ions mean more ejected atoms from the target, therefore, increasing the efficiency of the sputtering process. The magnetron allows to maintain the discharge for lower working pressure, therefore improving the quality of coatings.

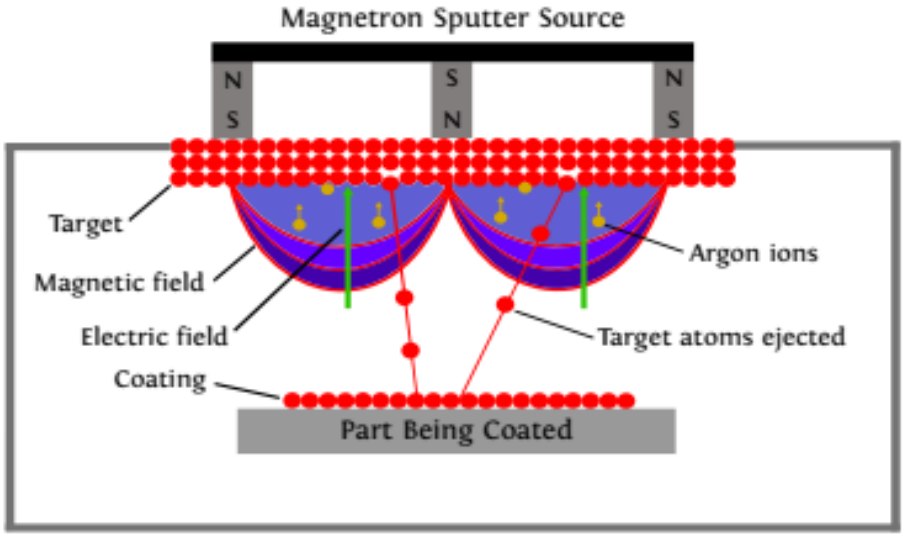

Figure 2. 2*:* Scheme a magnetron sputtering system. Figure extracted from [79]

2.2.3 Orion Sputtering Systems

Most of the films presented in this thesis have been deposited using the sputtering technology. To do so two Orion System built by AJA International with the same characteristics have been used. A brief overview of the capabilities of this system will be presented here. The system is a 8-target sputtering system using planar magnetron sources improvement. The particular

configuration of the sources enclosed in a chimney with narrow source shutter gap minimizes the cross contamination between sources. Both RF, DC and DC-pulsed regime can be used to generate the plasma and the several power supply allow the co-deposition of materials. The system can handle substrates up to 4 inches in diameter and the substrate holder allow simultaneous, rotation, heating, RF bias (for in-situ substrate pre-cleaning) and deposition at up to 850 °C in suitable sputtering environment (600 °C in a pure Oxygen environment). Stability is to within ± 1-degree C, Deposition uniformity over 4" is better that ± 2% and temperature uniformity is better that ± 1 %. A load lock chamber and cassette allow the samples to be removed and changed without venting the chamber. The cassette can hold up to 6 substrates holders and up to 4" wafer sizes can be accommodated in the system. Pumping of the main chamber are thanks to a turbo-pump (capable of pumping O2) control independent of gas flow. Flow rates controlled with standard mass flow controllers. Argon is used for the sputter gases, with N_2 and O2 used for reactive sputtering. The system is recipe driven and computer controlled for reproducible results.

Figure 2. 3*:*AJA International magnetron sputtering system used to grow Gd thin films.

Deposition conditions

All samples were prepared on glass substrates using dc-powered sources from pure elemental targets of 2" diameter. The chamber was evacuated with a set of rotary and turbopump to below 10^{-7} Torr prior to sputtering and the Ar gas pressure during sputtering was typically 10^{-3} Torr. The calibrated and the rotation speed (= 40rpm) of the substrate.

2.3 Structural Characterization

- **X-Ray Diffractometry**

The structural characterization of the deposited films was performed by X-ray diffraction. Since the X-rays wavelength is comparable to the interplanar distances in crystalline materials, X-ray diffraction is a very useful technique to: detect the crystallinity/amorphization nature of the sample and help to identify the crystalline phases present in the sample (bulk and thin film).

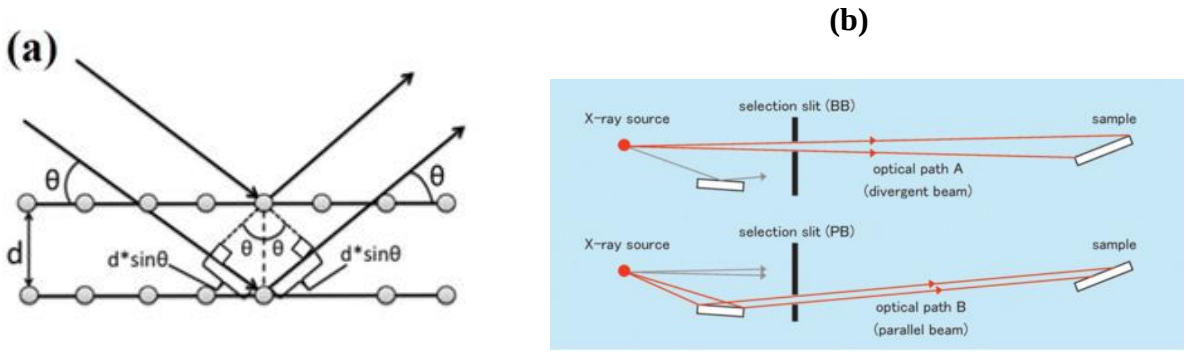

Figure 2. 4 ***:a)*** Schematic representation of Bragg Law, where the parallel lines represent the atomic planes which are separated by a distance, d, and the orange waves illustrate the incident and diffracted X-ray beam with wavelength, λ. **b)** Representation of Bragg Brentano (up) and the Parallel (down) X-ray beams, as extracted from reference [80].

The diffraction principle is pictured in Figure 2.4 **a)**. As can be seen, each atom in a periodic lattice scatters X-rays waves and when these waves add coherently it gives rise to a diffraction pattern with minima and maxima intensities. As Bragg stated, if we imagine a crystal as a set of planes of atoms then in order to have constructive interference, the difference of paths that

the X-rays (accounting for incident and scattered paths) travel has to be equal to an integral multiple of the wavelength. This was summarized in the formal expression of the Bragg law:

$$2d_{hkl}sin\theta = n\lambda \quad (2.1)$$

where $2d_{hkl}$ represents the distance of the family of atomic planes normal to the *hkl* direction [80]. Consequently, a family of atomic planes *hkl* will be responsible for an intensity peak at some specific angles θ_i and vice-versa i.e. the spacing between atomic planes determines the peak positions in the θ axis. A basic Diffractometer is constituted by four major parts: the X-ray source (typically its Copper) at the incident side, X-ray detector at the detector side, sample-holder/goniometer at the middle and the connection to a PC with the proper data acquisition software. The X-ray source is composed by a tube with one or more windows (that are transparent to X-rays), vacuum isolated, which has a W filament in one end and a target (typically Copper) at the other. When heating the filament, electrons are extracted from the W material and are accelerated by an electric field (in the 30-50 kV range, typically) towards the target (typically Copper). Some of these electrons cause abrupt transitions in the Cu atoms, which emit electromagnetic radiation with well defined wavelength in the 0.1-50 Å range - X-rays. The X-rays that hit the sample surface are required to be monochromatic and focused on the sample region which is attained through an optical system composed by several elements as monochromators and slits. Two geometries are mostly used: the Bragg Brentano (for bulk/powder sample diffraction) and Parallel Beam (for thin films). As can be seen in Figure 2.3, in the Bragg Brentano (BB) the X-ray beam is divergent with a determined solid angle that can be tuned by slits along its optical path, whereas the in the Parallel Beam (PB), as the name says, both the incident and diffracted beams are parallel. The PB geometry although typically less intense, does not depend critically on the sample position, morphology or shape due to their parallel waves nature, hence being particularly suitable for the thin film diffraction [80].

In this study, structural analysis were performed on a Bruker D8 Discover diffractometer (Nanotechnology Platform, MAScIR Foundation. Figure 2.5) under $CuK_\alpha 1$ radiation (λ=1.5406 Å) at room temperature, scanning angle 2θ ranging from 10° to 100° with a step of 0.1°. The objective of this analysis is the determination of the phase present in the samples and verification of the absence of secondary phases.

Figure 2. 5 *:* Bruker AXS X-ray diffraction system

2.4 Magnetic Measurements

Magnetic measurement are essential in characterizing the magnetic properties of materials used for various modern application. However, the technique that is best suited to any given application depends critically on the materials that are being measured, the parameter space (field, temperature, orientation of the field with respect to the sample) over which measurement are to be performed, as well as practical consideration (sensitivity, measurement speed). During this thesis we mostly used two characterization tools that allow for a quick but useful insight on the properties if our materials: VSM and MPMS magnetometry. The principals of the two will be qualitatively described here.

2.4.1 Vibrating Sample Magnetometry

In order to extract magnetic parameters as the effective anisotropy, the magnetization at saturation or the coercive field, the most widespread technique is the VSM (vibrating sample magnetometer) [81]. The principle of the measurement is to make the sample oscillate close to a coil. The coil feels an oscillating magnetic field associated to the local magnetic moment of the sample measured. This oscillating field induces a current in the coil that is proportional to the flux in the loop of current. By measuring the resulting voltage in the coil, it is then

possible to obtain the flux and consequently the magnetic moment of the sample. We can thus obtain in-plane or out-of-plan hysteresis loops by applying external fields to the sample. Different models of VSM exist, depending on the detection threshold wanted. The more precise one is a SQUID VSM, with an empirical detection limit in the range of 10^{-8} emu suitable for instance for measurements of ferrimagnetic samples. We measured hysteresis loops for ferromagnetic samples and using PPMS (property measurement system) VSM that has a detection threshold in the range of 10^{-6} emu. This PPMS VSM works also in a range of temperature from 1.9K to 400K and it can be used to performed M(T) measurements from which we can extract the Curie temperature of a sample. Hysteresis loops have been performed Nancy using 7T Magnetic Properties Measurement System (shown in figure 2.6)

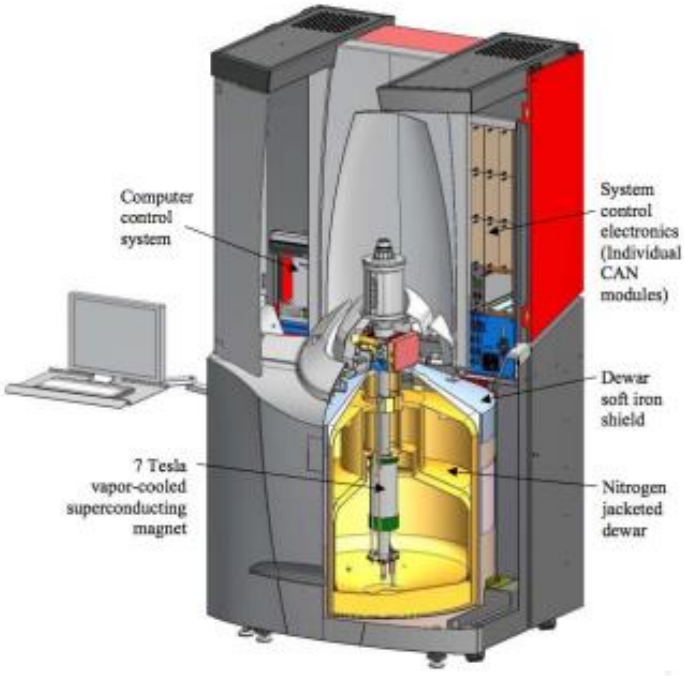

Figure 2. 6 :Schematic of the 7 T Magnetic Properties Measurement System SQUID-VSM I used in Nancy to perform isothermal magnetization M(H) measurements.

2.4.2 Types of measures

Different types of measurements have been performed to probe different material properties. The measurements that will be explained in the following are the measurements of

magnetization as a function of temperature **(M vs T)**, magnetization as a function of the applied magnetic field **(M vs H)** and finally, the measurements to determine the magnetocaloric effect.

- **M Vs T**

Temperature-dependent magnetization measurements allow to determine the ferromagnetic-paramagnetic transition temperature of the samples. They can also be used to determine whether it is an ordered or disordered phase, the phase with a transition temperature much lower than the ordered phase. To perform this measurement, a relatively weak magnetic field is applied at high temperature. The sample is then cooled under a magnetic field up to 10 K. The sample is centered and the measurement is carried out using the maximum magnetization. The temperature is scanned at a rate of 5˚C/min from 10 K to 400 K (see figure 2.7). The centering of the sample is modified between each measurement to take into account the thermal expansion of the straw moving the sample. Particular attention must be paid to the choice of the magnetic field at which the measurement is made. If the field is weaker than the coercive field of the material at low temperature, the curve can be greatly altered and may lead to misinterpretation of the results.

For example, when the field is too weak, there may appear to be a double transition characteristic of a sample with disordered and ordered phase. But by increasing the field slightly, the magnetization shows only an ordered transition. On the other hand, the higher the field is used, the more the magnetic transition is expanded in temperature. It is therefore necessary to use a magnetic field just higher than the coercive field at low temperature for a given material.

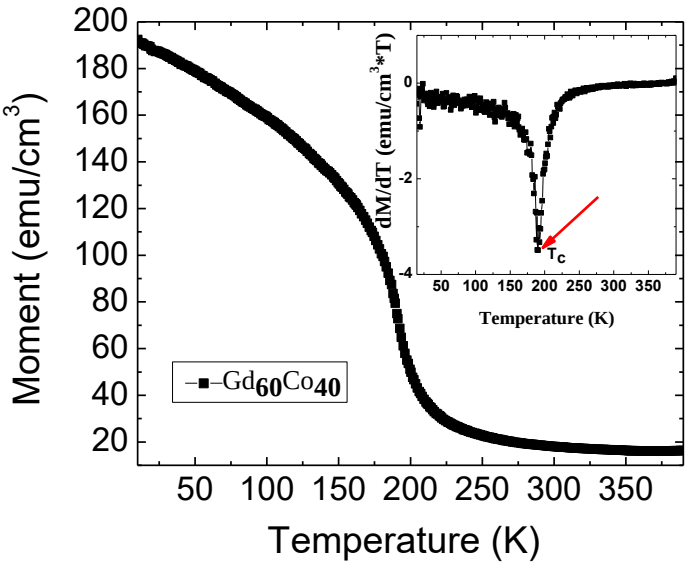

Figure 2. 7: Typical Temperature dependence of magnetization of $Gd_{60}Co_{40}$ alloy thin film as measured in a field of 500 Oe. Inset : First derivative of magnetization showing the Curie temperature (red arrow)

For example, when the field is too weak, there may appear to be a double transition characteristic of a sample with disordered and ordered phase. But by increasing the field slightly, the magnetization shows only an ordered transition. On the other hand, the higher the field is used, the more the magnetic transition is expanded in temperature. It is therefore necessary to use a magnetic field just higher than the coercive field at low temperature for a given material.

- **M Vs H**

The measurements of magnetization as a function of the magnetic field (M vs H) allow to determine the coercivity (H_c), the saturation magnetization (M_s) at a certain temperature. The measurements were performed at 5 K to obtain the maximum values of H_c and M_s. During a typical measurement, the magnetic field is varied by -2 T at 2 T and returned to -2 T. Measurements are made after the field is stabilized at the desired value. The field is varied at

regular intervals by decreasing the step in low field magnetic field to properly identify the coercive field and magnetization slash. As the temperature is kept constant, the measurement is carried out in using the maximum slope technique. This measure is important because it has a series of substrates produced by the supplier Crystec was found to possess an unusual magnetic character at low temperature, which skewed the interpretation of the M vs T data. It also makes it possible to make good measurements of M vs T in circumventing problems related to the coercive field.

When measuring the magnetocaloric effect on the materials produced, several problems have been encountered, most of which are related to the weakness of the magnetic moment of the layer in relation to the substrate and the straw of the specimen holder. A particular sequence was then developed to limit experimental errors. First of all, the measurement consists of magnetic field scans from 0 to 2 T at different temperatures around the magnetic transition temperature of the material. Since materials may have other magnetic transitions, such as for the phase disordered for example, the measurements were made from 10 K `to 320 K every 10 K except around the transition where the temperature varies with a 4 K step from 50 K below the transition to 50 K above the transition. Since each M vs H curve is performed at constant temperature, the technique of measuring the maximum slope was used.

- **Magnetocaloric Measurements**

The two characteristics of magnetocaloric material, ΔS_M and ΔT_{ad}, can be determined either directly or indirectly. Direct isothermal measurement of the heat transfer and, therefore, direct measurement of ΔS_M is inconvenient and it is rarely performed in practice. For the measurement of ΔT_{ad}, both direct and indirect methods are straightforwardly employed. A number of parameters affect the accuracy of such measurement of ΔT_{ad}, among which are the thermal contact between the sample and the temperature sensor, and the influence of external field on the temperature sensor. Therefore, the measured ΔT_{ad} is generally smaller than real value.

The majority of the characterization of the MCE is based on Eq. (1.9), which can be used to calculate ΔS_M indirectly from experimentally measured magnetization as a function of temperature and field. Isofield measurement determines the critical temperature, thermal hysteresis, and the width of the transition. Isothermal measurement is used to calculate the isothermal magnetic entropy change using the Maxwell relations. Both measurements probe the same phenomenon, and therefore should be equivalent.

In an isofield measurement, the sample is brought down to a temperature where the phase is completely magnetic (ferromagnetic in our case) without any external field. Then a small field (typically 0.05 T) is applied and the magnetic transition is probed continuously at constant field while ramping up the temperature until the phase is completely paramagnetic. A cooling curve under the same field is often applied to determine any thermal hysteresis.

As for an isothermal measurement, the usual procedure is to start in zero field at a given temperature (typically T_C -50 K), ramp the field from 0 to H_f (2 T) in discrete steps while recording the magnetization (see Figure 2.8(a). At each step the magnetization is measured with fixed temperature and field. Once H_f is reached the field is brought back to zero and the temperature is increased by a discrete step and the process of increasing field is repeated. This is repeated for every temperature until the maximum temperature (T_C + 50 K) is reached.

From these isothermal measurements (Figure 2.8 b), the isothermal magnetic entropy change can be calculated by integration of the Maxwell relation Eq.(1.9). Because the measurements are made at discrete temperature intervals, ΔS_M can be numerically calculated using

$$\Delta S_M(T, \Delta H) = \mu_0 \sum_j \frac{M\left(T+\frac{\Delta T}{2}, H_j\right) - M\left(T-\frac{\Delta T}{2}, H_j\right)}{\Delta T} \Delta H_j \qquad (2.2)$$

Where ΔH is the sum of ΔH_j, $M\left(T+\frac{\Delta T}{2}, H_j\right)$ and $M(T-\frac{\Delta T}{2}, H_j)$ represent the value of the magnetization in a magnetic field H_j at the temperature $T+\frac{\Delta T}{2}$ and $T-\frac{\Delta T}{2}$ respectively.

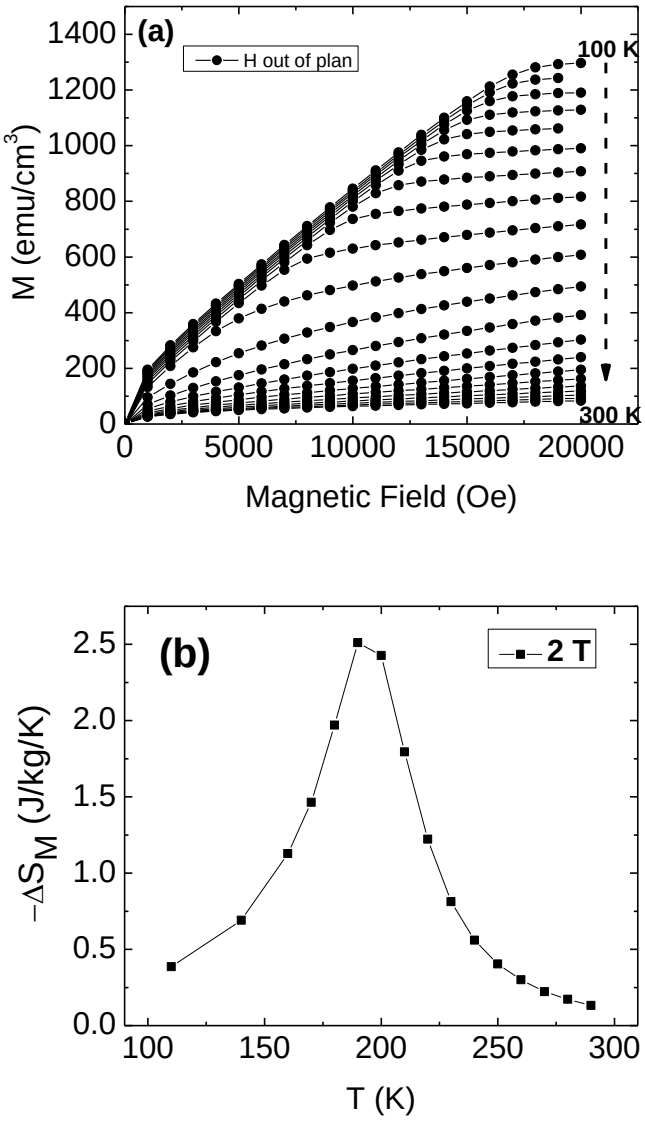

Figure 2. 8 : (a) magnetization versus field curve (H = 0 – 2 T) for $Gd_{60}Co_{40}$ over the temperature region around T_c **;(b)** Magnetic entropy change in for $Gd_{60}Co_{40}$ alloy thin film

The data were calculated from magnetization data recorded on increasing and decreasing magnetic fields.

It might also be useful to note that the measured entropy change is smaller than the total entropy change associated with a transition from full disorder to total order. The difference comes from the dynamics of ordering processes in condensed matter. Just above T_C, the ferromagnetic state still has long range order, but the magnetization is reduced due to thermal excitation. As the transition passes just above T_C, there still remains short range order. Therefore, the entropy change is not really changing from an "on" state to an "off" state.

- **Refrigerant Capacity (RC) and Relative Cooling Power (RCP)**

While it is clear that the magnitude of ΔS_M at its peak is important to the overall refrigeration capabilities of a material, this value is only valid for a single temperature; generally, at or near the Currie temperature. In practice, however, one would need to know the magnetocaloric behavior in the entire temperature region of a working device. Where the operating temperature is taken to be the temperature range starting at the temperature which represents ΔSM at 50% of the maximum on the low temperature side of the peak, and continuing on to that same value of ΔS on the high temperature, this is generally referred to as the full width at half maximum (FWHM). There are several figures of merit used to describe the overall capabilities of a magnetocaloric material; notable are the refrigerant capacity (RC) and the relative cooling power (RCP). RC is taken to be the integral under the $\Delta S_M(T)$ curve for a given field change, integrated from one reference temperature to another. This is illustrated in Fig. 2.4 as a solid blue shaded area with reference temperatures corresponding to the FWHM.

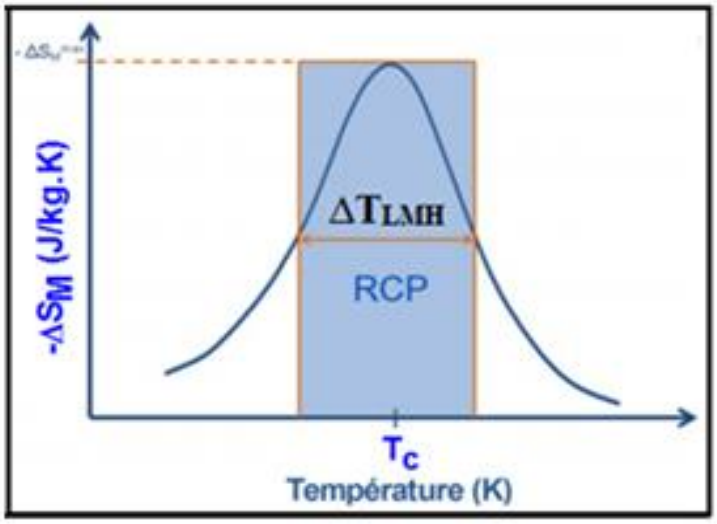

Figure 2. 9 The colored dots correspond to the refrigerant capacity is the shaded area under the 2 T field change curve; the relative cooling power is the area of the rectangular box.

The formal definition is as follows:

$$RC = \int_{T_2}^{T_2} -\Delta S_M(T)dT$$

where T_1 and T_2 are the reference temperatures on the low and high temperature side of the peak respectively. Because this integration results in units of power (J/kg), it becomes a useful figure of merit when comparing to other sources of refrig eration. While RC works well when analyzing MCE materials when one has access to all of the raw data, it is not very useful for comparing one's own results to others who have not reported on this figure of merit. In this case an estimation of the integral can be useful, and is generally referred to as RCP. To estimate the integral quickly from reported MCE data, one can simply multiply the ΔS_{max} value by the FWHM. While this still gives units of power (J/kg).

Chapter 3:

Magnetocaloric Effect in $Gd_{100-x}Co_x$ Thin Films and Heterostructures

Part 1 Magnetic Properties and Magneto-Caloric Effect in $Gd_{100-x}Co_x$ Thin Films

3.1.1 Introduction

The study of the magnetocaloric effect as a means for magnetic cooling has attracted rising interest due to the prospect of replacing conventional refrigeration systems [82,83]. Recently, various experimental and theoretical works have been carried out on magnetic materials showing a large magnetocaloric effect [84,85]. Moreover, many studies of the magnetocaloric effect (MCE) for ambient applications have been performed on rare-earth based compounds, since the latter show high magnetic moments. However, the MCE was found to be rather small for this class of material. Indeed, the largest MCE was reported for the rare-earth element Gd, where the ΔSM value goes up to $-9.8\ Jkg^{-1}K^{-1}$ and ΔT_{ad} near $T_c = 293$ K is about 11.6 K for a magnetic field change of 5T [86]. In 1997, Pecharsky and Gschneidner demonstrated in their pioneering work a giant MCE in the compound $Gd_5Si_2Ge_2$ [87], a discovery that reawakened interest in magnetic refrigeration for ambient applications. Later, several different classes of materials were found to exhibit giant MCEs near room temperature, such as $MnAs_{1-x}Sb_x$ [88], $La(Fe_{1-x}Si_x)13$ [89] and their hydrides [90], $MnFeP_{1-x}As_x$ [91], as well as $Ni_{0.5}Mn_{0.5-x}Sn_x$ [92]. However, most these investigations were limited to the investigation of the MCE in bulk materials, while works on magnetic thin films are very limited.

Recently, the study of the MCE in thin films has triggered more interest, namely the study of Gd/W multilayers [93,94], manganites [95,96], FeRh [97], NiMnGa [98], and MnAs [99]. From a technological point of view, the use of magnetic refrigerant in the form of thin films, powders, or wires is more desirable [86,100,101 ,102]. In this context, many magnetic coolers based on Gd powders and laminate structures were demonstrated [82]. More recently, many studies have investigated the effect of the dimensionality reduction on MCE parameters [94,103,104,105]. Indeed, it was recently reported that the reduction of dimensionality in a ferromagnetic material broadens the paramagnetic to ferromagnetic (PM-FM) transition, shifts it to lower temperatures, and also reduces the magnetization saturation and magnitude

of (ΔS_M) [103]. On the other hand, the broadening of (ΔS_M) in thin films should enhance the relative cooling power (RCP), which is preferable for magnetic refrigeration. In this work, we have investigated the impact of the substitution of gadolinium with cobalt in thin film form on the magnetic and magnetocaloric properties of $Gd_{100-x}Co_x$ alloys. We have developed and optimized the magnetic properties of $Gd_{100-x}Co_x$ thin film alloys deposited by sputtering techniques, and then derived temperature dependence of the entropy change [106].

3.1.2 Experimental method

The thin films were deposited at room temperature on (100)-silicon substrates by the sputtering deposition technique. The chamber base pressure was 10^{-7} Torr. A 3 nm-thick Ta layer was used as a buffer layer, while a 3 nm-thick Ta capping layer was used to prevent the oxidation of the rare-earth elements. The deposition rates for Gd and Co targets at 50 W and 100 W were 0.719 Å/s and 0.456 Å/s, respectively. The thickness of $Gd_{100-x}Co_x$ ($40 < x < 56$) alloy films was kept constant and equal to 100 nm in order to ease the comparison of the magnetocaloric values. The magnetic characterization was carried out using a Quantum Design© SQUID-VSM, where the magnetic field is applied in the sample plane.

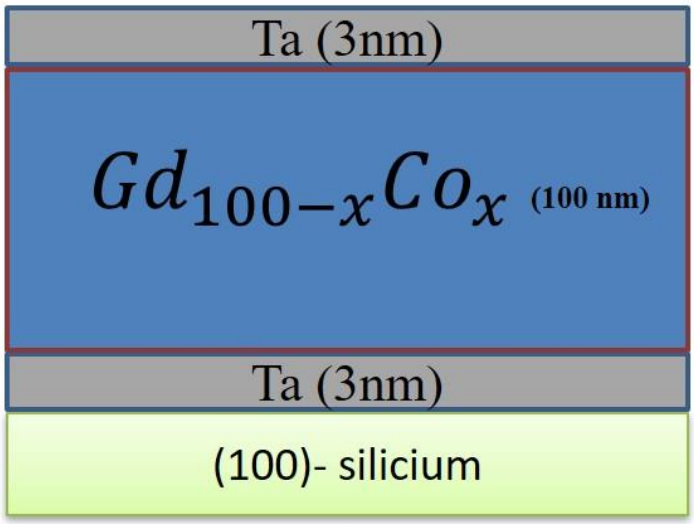

3.1.3 Structural characterization

Figure 3.1 shows the XRD pattern for the $Gd_{48}Co_{52}$ and $Gd_{56}Co_{44}$ alloy thin film. The $Gd_{56}Co_{44}$ thin film is fully amorphous, while the $Gd_{48}Co_{52}$ thin film contains plenty of crystalline peaks around 35°.

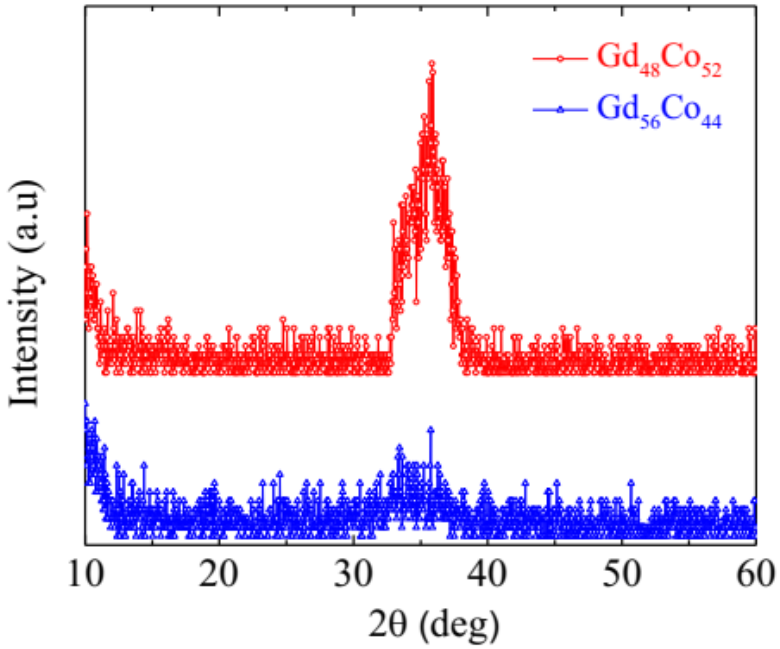

Figure 3. 1*:* The XRD patterns of $Gd_{100-x}Co_x$ alloy are in the figure.

3.1.4 Magnetic properties

We measured the temperature dependence of magnetization for all the studied alloy films to determine the temperature as well as the nature of the transition. figure 3.2**a** show the temperature dependence of the magnetization obtained under an applied magnetic field of 500 Oe for $Gd_{100-x}Co_x$ alloy films with different Co concentrations x = 56, 52, 48, 44, and 40. The PM-FM transition temperature Tc shown in the inset corresponds to the minimum of dM/dT. The obtained values for Tc are 190 K for $Gd_{60}Co_{40}$, 205 K for $Gd_{56}Co_{44}$, 240 K for $Gd_{52}Co_{48}$, 282 K for $Gd_{48}Co_{52}$, and 335 K for $Gd_{44}Co_{56}$, respectively. It can be clearly seen from figure 3.2b that the T_c of the studied $Gd_{100-x}Co_x$ alloy films increases as a function of the Co concentration *x*, which is mainly due to the strong Co–Co ferromagnetic exchange interaction.

Indeed, any nearest neighbor of Co interacts ferromagnetically regardless of the crystal structure [107].

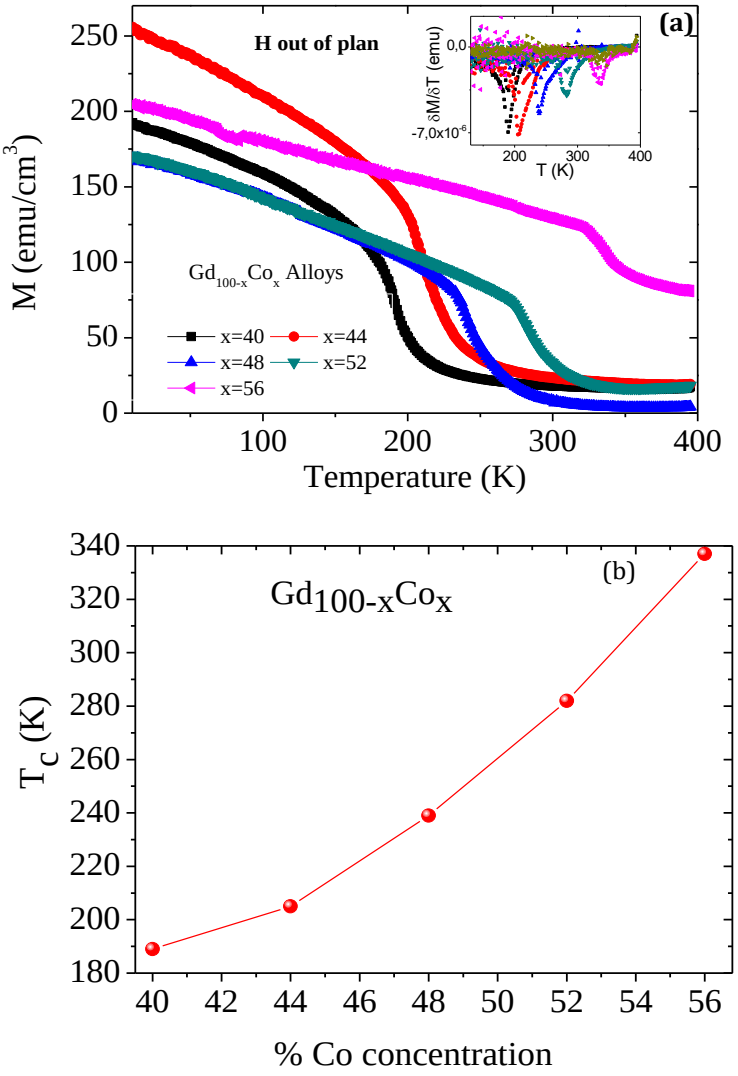

Figure 3. 2: (a) Temperature dependence of magnetization in the Gd100-xCox for various compositions under an applied field of 500 Oe. The inset shows the derivative curves of dM/dT vs T. (b) the relationship between the Tc and the Co concentration x

As we know, the first order transition materials inevitably have hysteretic losses, which would lower the magnetic refrigeration. It has attracted some research interest in how to depress the magnetic hysteresis of the first order transition materials recently [146]. As for the second order

transition magnetic materials, they often present no thermal hysteresis and reduced magnetic hysteresis. Figure 3.3 shows the typical magnetic hysteresis loop of $Gd_{48}Co_{52}$ alloy thin film measured at 5 K, which is below tis T_c. it almost saturate under the magnetic field of 20 kOe with a saturation magnetization (M_s) of about $1.1*10^4$ emu/cm^3. It is assumed that the large magnetization mainly results from the magnetic moment of Gd atoms [147] since Gd ions is an S-state ion and has negligible field anisotropy in Gd-rich alloys [148]. From the inset of Figure3.3, we can observe that the coercivity of $Gd_{48}Co_{52}$ alloy thin film is only about 40 Oe, which means that the hysteresis loss would be reduced remarkably, during the magnetization and demagnetization process in the refrigeration cycle.

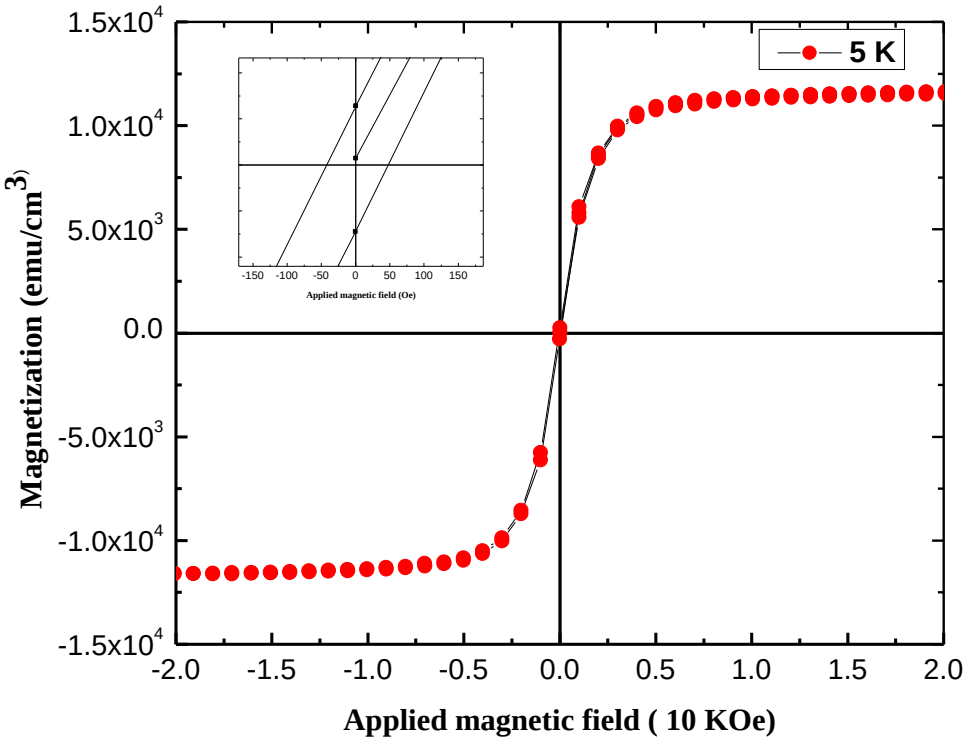

Figure 3. 3 : Magnetic hysteresis loops of *$Gd_{48}Co_{52}$* alloy thin film at 5 K, the inset shows the coercivity field.

3.1.5 Magnetocaloric effect properties

Figure 3.3a shows isothermal magnetization M (H) curves measured for $Gd_{56}Co_{44}$ alloy film under an applied magnetic field up to ΔH = 20 kOe and a temperature ranging from 150 to 290 K. The magnetization curves below the T_c show a non-linear behavior with a tendency towards saturation under the applied magnetic field, which indicates a ferromagnetic behavior. However, the magnetization above the T_c shows a linear behavior, which reflects a paramagnetic behavior. The latter is due to the thermal agitation which disarranges the magnetic moments. In order to determine the nature of the transition in $Gd_{56}Co_{44}$ alloy film, we used the Arrott plot method and employed the Inoue-Shimizu model [108]. According to the Banerjee criteria [109], the positive (resp. negative) slope of the M^2 (H/M) curves indicates a second- (resp. first-) order transition. As shown in Figure 3.3b, only positive slopes of the M^2 (H/M) curves were observed for the $Gd_{56}Co_{44}$ alloy film, indicating that the PM-FM transition is a second order transition.

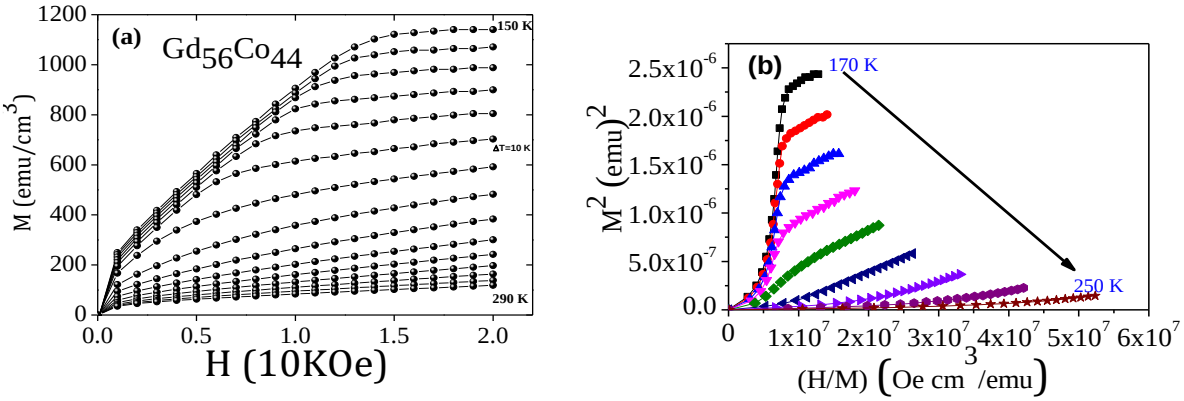

Figure 3. 4: **(a)** Magnetization isotherms curve and **(b)** the Arrot plots of isotherms in the vicinity of T_c of $Gd_{56}Co_{44}$ alloy compound

Based on the magnetization curves reported in Figure 3.3 (a), the isothermal magnetic entropy change caused by the variation of the external magnetic field from 0 to $\Delta H = 20kOe$ can be determined by using the well-known Maxwell relation :

$$\Delta S_M(T, H_0) = \mu_0 \sum_i \frac{M_{i+1}(T_{i+1}, H) - M_i(T_i, H)}{T_{i+1} - T_i} \qquad (3.1)$$

We compared the values of $-\Delta S_M$ obtained for the investigated $Gd_{100-x}Co_x$ alloys with x = 56, 52, 48, 44, and 40 with those obtained for a 100 nm-thick Gd layer, as depicted in figure 3.4.a. The maximum values of the $-\Delta S_M^{Peak}$ (T) curves are obtained close to T_c. The peak temperature in $-\Delta S_M$ (T) is shifted towards high temperature by increasing x, which is most likely due to the enhancement of the Gd–Co indirect interaction. Figure 3.4.b shows the evolution of the peak entropy change value and its full width at half maximum (FWHM) as a function of the Co concentration *x*. It can be clearly seen that the decrease in peak $-\Delta S_M$is accompanied by an increase of the FWHM. The maximal entropy change is observed for *x* = 44, and is about 2.65 J/kg.K. Figure 3.4c shows the evolution of $-\Delta S_M^{Peak}$ as a function of $T_C^{-2/3}$ for the investigated $Gd_{100-x}Co_x$ alloys (x = 40, 44, 48, 52, 56) under the applied magnetic field of 2 T. It can be seen from figure 4.4b that$-\Delta S_M^{Peak}$ changes linearly with $T_c^{-2/3}$ (or $(708.8–8.83x)^{-2/3}$ with a linear correlation coefficient above 0.992), indicating that $-\Delta S_M^{Peak}$ of the $Gd_{100-x}Co_x$ alloys can be easily tailored by adjusting *x*.

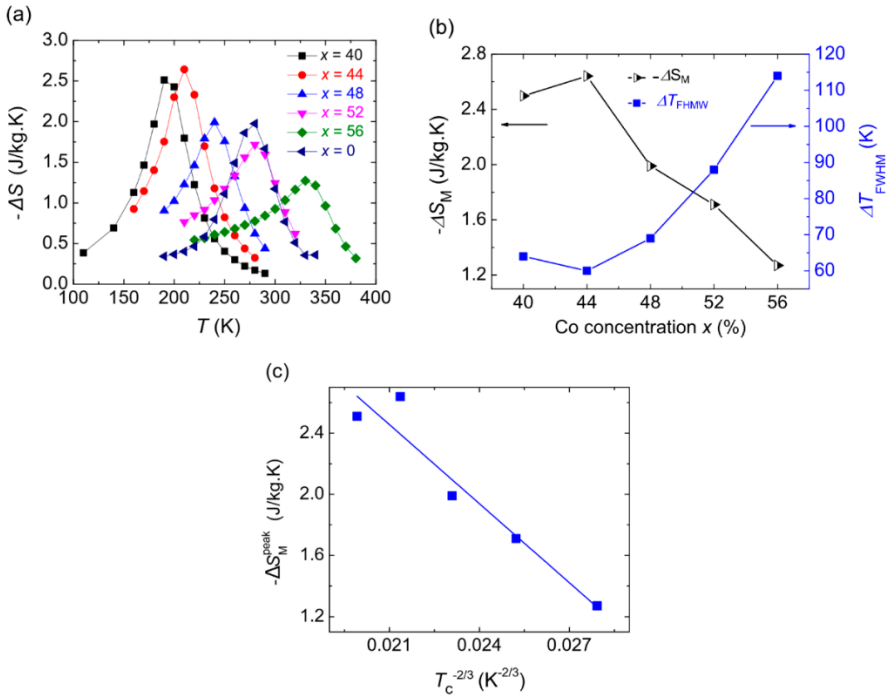

Figure 3. 5 *:* **(a)** Temperature dependence of the magnetic entropy change, **(b)** co-concentration dependence of the magnetic entropy change peak and the full width at half maximum (FWHM) of $-\Delta S_M$ (T) peak, and **(c)** the dependence of $-\Delta S_M^{Peak}$ as a function of $T_c^{-2/3}$ for the studied Gd100−xCox alloys compounds under an applied magnetic field of ΔH = 20 kOe.

In addition to the isothermal entropy change, the relative cooling power (RCP) is also a key parameter to evaluate the magnetocaloric performance. The RCP considers both the isothermal magnetic entropy change and the working temperature range of magnetocaloric materials, and it is given by the following formula:

$$RCP = -\Delta S_M \times \delta T_{FWHM} \quad (3.2)$$

where T_{FWHM} is the full width at half maximum obtained from the temperature at half the maximum peak value of the $-\Delta S_M$ curve. Figure 3.5 shows the evolution of the RCP of the $Gd_{100-x}Co_x$ thin films as a function of the applied magnetic field. The RCP value increases with the applied magnetic field. Moreover, all the studied $Gd_{100-x}Co_x$ alloys present a large RCP value around 140 J/kg for ΔH=20 kOe, which is significantly higher than the RCP of the Gd thin films. Table 1 shows a summary of the present results, the MCE properties of the GdCo thin films, as well as some others reported in the literature. The high values of the RCP and $-\Delta S_M$ (T) obtained for the $Gd_{100-x}Co_x$ thin film alloys is very promising for magnetic refrigeration applications with a wide temperature range.

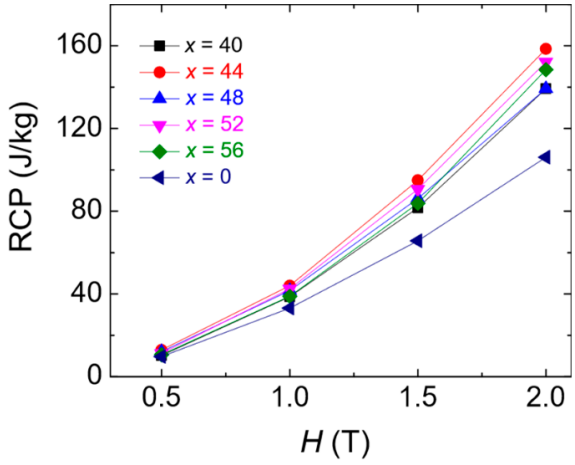

Figure 3. 6 *:* Relative cooling power (RCP) as a function of the applied magnetic field for the $Gd_{100-x}Co_x$ alloy films

Materials	T_c (K)	$-\Delta S_M^{peak}(J/kg.K)$ $\Delta H = 20kOe$	$RCP(J/kg)$ $\Delta H = 20kOe$	ΔH (T)	Referen-ces
$Gd_{60}Co_{40}$	190	2.51	139	2	This thesis
$Gd_{56}Co_{44}$	205	2.64	158	2	This thesis
$Gd_{52}Co_{48}$	239	1.99	139	2	This thesis
$Gd_{48}Co_{52}$	282	1.71	152	2	This thesis
$Gd_{44}Co_{56}$	337	1.27	148	2	This thesis
Gd_{100}	280	1.97	106	2	This thesis
$Gd_{71}Co_{29}$ amorphous ribbons	166	3.1	92.3	1	[111]
$Gd_{62}Co_{38}$ amorphous ribbons	193	2.8	81.4	1	[111]

Table 3. 1 *:* Magnetic and magnetocaloric properties of $Gd_{100-x}Co_x$ compounds with variation in Co doping

3.1.6 Universal Scaling Analysis

Universal scaling analysis indicates that the Co helps to homogenize the magnetic properties in GdCo thin films [106]. Such a method should remove the temperature and field dependence of the set of ΔS_M $(\Delta H, T)$ curve (for fixed ΔH), so that all curves processed with the same scaling protocol collapse onto a single universal curve. A failure to display this universal collapse can be attributed to material inhomogeneity [111], likely

in the form of a distribution of exchange energies. Figure 3.6 shows the universal curve construction for each of the studied $Gd_{100-x}Co_x$ thin films by plotting ΔS′ against θ, where $\Delta S' = \frac{\Delta S_M}{\Delta S_M^{Peak}}$ is the rescaled entropy change and θ is the rescaled temperature variable as follows:

$$\theta = \begin{cases} -(T - T_C)/(T_{r1} - T_C) & T \le T_C \\ (T - T_C)/(T_{r2} - T_C) & T \ge T_C \end{cases} \tag{3.3}$$

with T_{r1} and T_{r2} are reference temperatures chosen at 50% of ΔS_{Max} above T_c . As shown in Figure 4.6, the curves do not collapse into one single curve. Moreover, one can see from figure 4.6 that the degree of collapse increases with the Co concentration. It has been shown that a failure to collapse (such as seen for x = 44) can be attributed to inhomogeneity within the material.

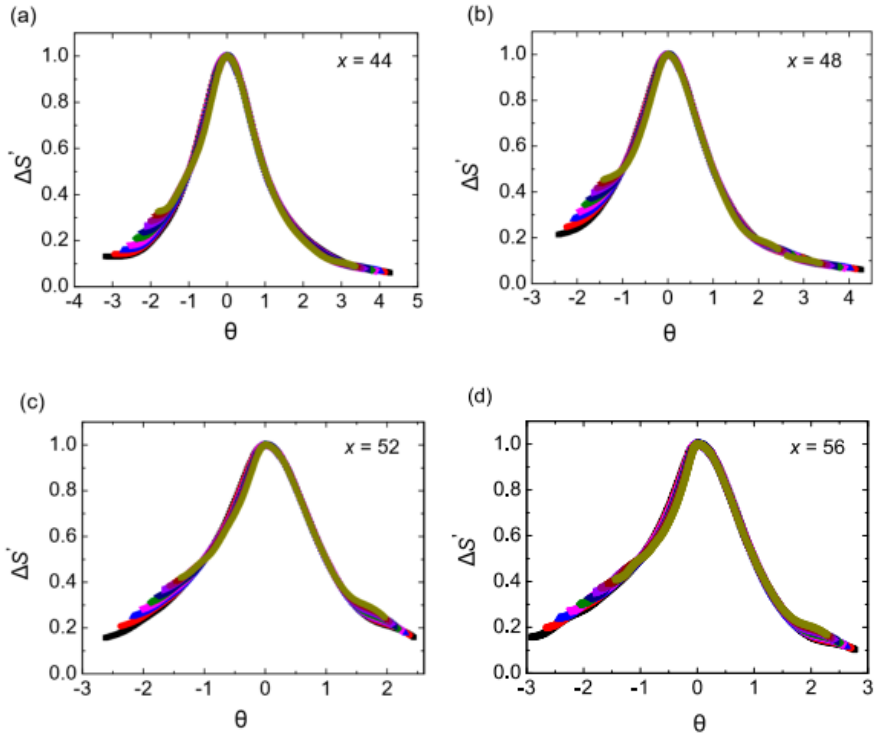

Figure 3. 7 *:* The normalized entropy changes as a function of the rescaled temperature θ for different applied fields for $Gd_{100-x}Co_x$ **(a)** x = 44, (b) x = 48, (c) x = 52 and (d) x = 56 thin films.

3.1.7 Critical Exponents

The second-order transition FM to PM near the Curie point is characterized by a set of critical exponents: β correspond to spontaneous magnetization, γ relevant to the initial susceptibility, and δ correspondent to the critical magnetization isotherm at Tc. Possess the following power-law dependences[112]:

$$M_s(0,T) = m_0 |\varepsilon|^{\beta}, \qquad \varepsilon \leq 0 \tag{3.4}$$

$$\chi_0^{-1}(0,T) = \frac{h_0}{m_0} |\varepsilon|^{\gamma}, \qquad \varepsilon \geq 0 \tag{3.5}$$

where $\varepsilon = \frac{(T-T_C)}{T_C}$ is the reduced temperature, and m_0 and $\frac{h_0}{m_0}$ are the critical amplitudes. Initial values of β=0.4 and γ=1.33 are selected, then a plot of $M^{1/\beta}$ as a function of $(\frac{H}{M})^{1/\gamma}$ was obtained [12]. The high field linear region (H > 1) is used for the analysis, because the Modified Arrott Plots (MAPs) tend to deviate from linearity at low field due to the mutually misaligned magnetic domains. The values of M_s and χ_0^{-1} can be then determined from the intersection of the linearly extrapolated curves with the $M^{1/\beta}$ and $(\frac{H}{M})^{1/\gamma}$, respectively. Figure 3.7a show the temperature dependence of χ_0^{-1} (T) and M_s (T), which are fitted with Equations (3.4) and (3.5). The fitting enables us to obtain new values of β and γ, which are then used to construct new MAPs. These steps are therefore repeated until the iterations converge to the optimum values of β, γ, and Tc. Therefore, the MAPs shown in 3.7a yielded the following results: β=0.47±0.009 and γ=1.15±0.1. 3.7b depicts the modified Arrott plots, which show that all lines are parallel to each other. On the other hand, the fitting of the M-H measured at T close to T_C using Equation (3.6) enables to extract the value of the critical component δ:

$$H = DM^{\delta}, \qquad t = 0 \tag{3.6}$$

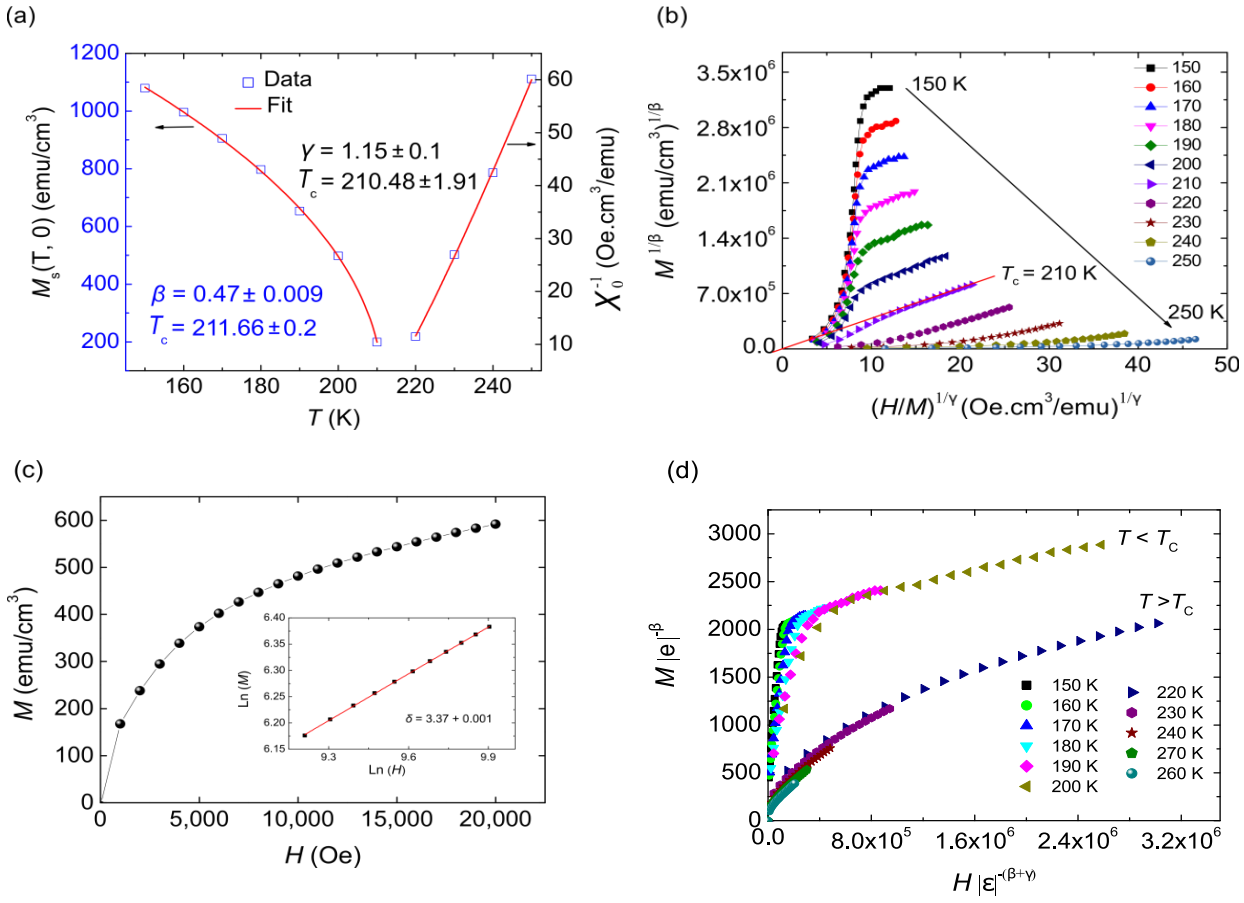

Figure 3. 8 *:* (**a**) Spontaneous magnetization and inverse of initial susceptibility vs temperature, (**b**) modified Arrott plot : isotherms of $M^{1/\beta} \sim (H/M)^{1/\gamma}$ with the calculated exponents, (**c**) isothermal M(H) plots with the log-log scale at T_c= 210 K, (**d**) scaling plot with $M(H,\varepsilon)\varepsilon^{-\beta}$ versus $H\varepsilon^{-(\beta+\gamma)}$ below and above Tc using exponent determined from the modified Arrott plot of $Gd_{56}Co_4$ alloy film.

Figure 3.7c shows the magnetic field dependence of magnetization at Tc for $Gd_{56}Co_{44}$ thin films. while the critical isotherm on a log–log scale is shown in the inset. The extracted value of 3.37 ± 0.001. δ can also be extracted via the Widom scaling relation [113]:

$$\delta = 1 + \frac{\gamma}{\beta} \tag{3.7}$$

By using the critical parameters β and γ obtained using the MAPs, the deduced δ value is 3.44. thus, the Widon scaling relation has confirmed the reliability of the critical exponents deduced from experimental data. The reliability of the calculated exponents β and γ can be confirmed by using the scaling hypothesis following:

$$M(H,\varepsilon) = \varepsilon^{\beta} f_{\pm}(H/\varepsilon^{\beta+\gamma}) \qquad (3.8)$$

Where $f_{\pm}$ are regular analytical functions with f_{+} and f_{-} for above and below Tc, respectively. The scaling relation claims that $M(H,\varepsilon)\varepsilon^{-\beta}$ versus $H\varepsilon^{-(\beta+\gamma)}$ should yield two universally different branche, one for $T > T_c$ and the other for $T < T_c$. Using the values of β ,γ and T_c from the MAPs method in figure 3.7(d). It is clear that all the magnetization data fall into two universal curves, one for temperature above Tc and the other for temperature below Tc, in agreement with the scaling theory. This therefore confirms that the obtained values of the critical components as well as the Tc are reliable and in agreement with the scaling hypothesis. The critical exponents determined for both thin films are similar to the theoretical values from the mean field model ($\boldsymbol{\gamma}$ =1.0, $\boldsymbol{\beta}$ = 0.5 and $\boldsymbol{\delta}$ = 3) [114]. We also analyzed the critical behavior of magnetic phase transition using arrot plots for $Gd_{100-x}Co_x$ (x = 40, 48,52 and 56), which follow the mean field model. Consistent with the existence of long-range ferromagnetic interaction thus, the critical behavior analysis in the vicinity of Tc demonstrates that the magnetism of the GdCo thin film is governed by long range nature of ferrimagnetism in this system.

3.1.8 Conclusions

In summary, thin films of $Gd_{100-x}Co_x$ alloy compounds were deposited on silicon substrate using sputtering techniques. The magnetic and magneto-caloric effect of $Gd_{100-x}Co_x$ (x =44, 48, 52, 56) thin films were investigated. The Curie temperature increase when the concentration of Cobalt element increases. The maximal magnetic entropy change of the samples reached a maximum at the Curie temperature. Under an applied magnetic field of 2 T, the value of is found to be 2.64 for x = 44, respectively. Moreover, the samples present an important relative cooling power “RCP” higher than 140 J/Kg which considered as a recommended parameter for

a wide temperature range in magnetic refrigeration application. Moreover, critical properties study on the second-order ferromagnetic transition of $Gd_{100-x}Co_x$ thin film demonstrate that the magnetic interaction around T_c can be described with the mean field model corresponding to long-range interaction.

Part 2 Engineered Gd-Co based multilayer stack to enhanced magneto-caloric effect and relative cooling power

3.2.1 Introduction

Recently, magnetic refrigeration based on the magnetocaloric effect (MCE) of magnetic materials possesses the potential to substitute conventional gas compression refrigeration, and has been a topic of great interest for minimizing environmental impact [115]. The basic requirement for magnetic refrigeration materials is a large isothermal magnetic entropy change (ΔS_M). However, several features are required for the application in magnetic refrigeration, such as the Curie temperature (T_C) in the vicinity of the working temperature, a large magnetic entropy change over the entire temperature range of range of the cycle, an almost zero magnetic hysteresis, a reasonable thermal conductivity coupled with large electrical resistance, and a large adiabatic temperature change [116]. Therefore, the relative cooling power (RCP) is indeed considered to be the most important factor for assessing the usefulness of a magnetic refrigerant material [117].

During the last decade, MCE has been investigated in a very wide spectrum of materials that include elemental metals [118], rare earth intermetallic [119], manganese oxide materials [120], Mn alloys [121], lanthanides and Heusler compounds [122], bulk Gd alloys [123], and thin films [124]. However, investigating MCE in materials at nanoscale remains a novel endeavor and an open challenge. Indeed, recent studies on $La_{0.7}Ca_{0.3}MnO_3$ compounds in various forms, ranging from bulk and nanoparticles to thin films, showed that reducing the dimensionality of the LCMO compound tend to broaden and shift the paramagnetic-ferromagnetic transition to lower temperatures, while decreasing the M_S and the magnitude of ΔS_M [125]. Other studies on Gd-based structures demonstrated that the MCE also depends on the size and dimension [126,127]. Indeed, it appears that the combination of interfaces, defects,

and lower size can explain the enhancement of MCE for low dimension samples. For instance, a maximum of entropy was observed in Gd/W multilayer [128]. A more recent study by Lambert et al. showed that MCE can be tuned by changing the concentration of 100 nm thick Gd-Tb alloys and multilayers [129]. Moreover, a recent publication has shown that the $Gd_5Si_{2.7}Ge_{1.3}$ thin film exhibits a large magnetic entropy change (ΔS_M = 8.83 J.kg^{-1}K^{-1} for ΔH = 50 kOe) and present a broader magnetic response in comparison with its bulk counterpart [130]. In this paper, we report on the successful enhancement of the RCP value through the engineering of Gd-Co alloys based multilayer stack.

3.2.2 Sample structure

The studied sample is a 100 nm-thick Gd-Co alloys-based multilayer stack, namely Ta (3 nm)/ [$Gd_{1-x}Co_x$/ $Gd_{1-y}Co_y$ /…] (100 nm)/Ta (3 nm). The studied sample is grown on a glass substrate at room temperature (RT) using sputtering deposition with base pressure lower than 10^{-7} Torr and an Ar pressure fixed at 3.0 mTorr. The composition gradients were achieved by adjusting the deposition rates from the two independent magnetron guns. Sputtering rates for Gd and Co targets at 50W and 100W were 0.719 A˚/s and 0.456 A˚/s, respectively, as determined by low-angle X-ray reflectivity measurements. The schematic of the sample structure is illustrated in figure 3.8. Indeed, the sample is made of four 25 nm-thick Gd-Co alloy layers, while the composition of each layer is different and varies linearly from x = 0.44 for the first layer (bottom layer) to x = 0.60 for the fifth layer (top layer). A 3 nm-thick Ta buffer layer was used, whereas another 3 nm-thick Ta capping layer was used to prevent sample oxidation. Magnetic measurements were carried out by a Quantum Design Squid Vibrating Sample Magnetometer.

3.2.3 Magnetic and magnetocaloric effect:

Figure 3.9 shows the temperature dependence of magnetization M under an applied magnetic field of 500 Oe for the studied Gd-Co based multilayer stack sample. A typical paramagnetic to ferromagnetic phase transition can be observed at T_c. In order to estimate the T_c, we have used the inflection point method as described by Moreno-Ramirez et al [50]. Following this, a

value of T_c=230 K can be determined from the minimum of the derivative of the magnetization $\frac{dM}{dT}$ as shown in the inset of Figure 3.9.

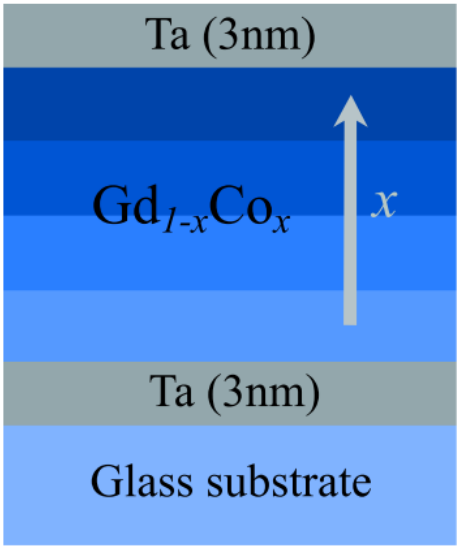

Figure 3. 9 *:* Sketch of the studied Gd-Co alloys based multilayer stack. The sample is made of four 25 nm-thick $Gd_{1-x}Co_x$, where Co concentration x increases linearly from 0.44 for the first layer (bottom layer) to 0.60 for the fourth layer (top layer).

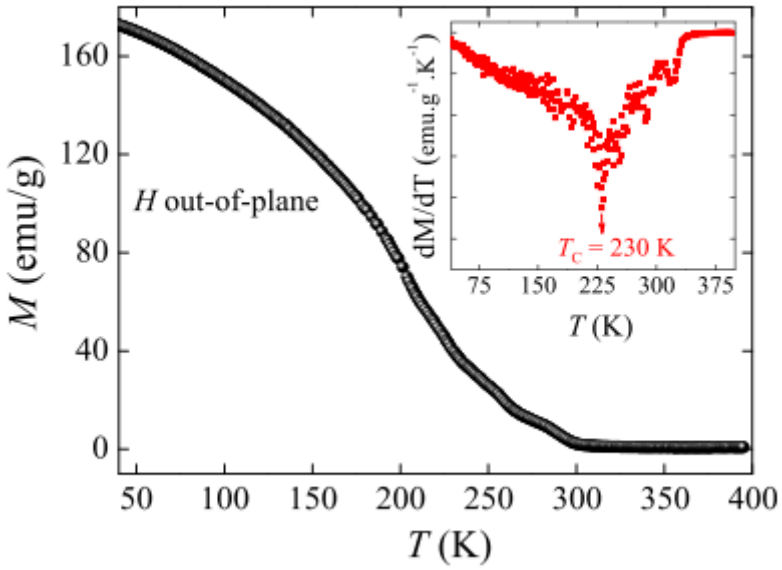

Figure 3. 10 *:* Temperature dependence of the magnetization under a magnetic field of 500 Oe for the studied Gd-Co based multilayer stack. The inset shows the evolution of $\frac{dM}{dT}$ as a function of temperature.

The magnetocaloric effect in the studied Gd-Co based multilayer stack was calculated from the isothermal magnetic entropy change $(-\Delta S_M)$ deduced from the magnetization versus magnetic field measurement performed a different temperature below and above T_c and in magnetic field up to 20 kOe. Figure 3.10 shows the temperature dependence of M obtained by sweeping the magnetic field from 0 to H_{max} using a sweeping speed of 250 Oe/s, with H_{max} = 10, 15 and 20 kOe, and for a temperature ranging from 60 to 400 K.

The isothermal magnetic entropy change $-\Delta S_M$ is equal to 1.55 $J.Kg^{-1}.K^{-1}$ for a magnetic field swept from 0 to 20 kOe. Figure 3.11 shows the Arrott plots derived from M (H) show a positive slop around T_c. According to the Banerjee criterion [132], this finding confirms that the measured paramagnetic-ferromagnetic transition is a second-order transition.

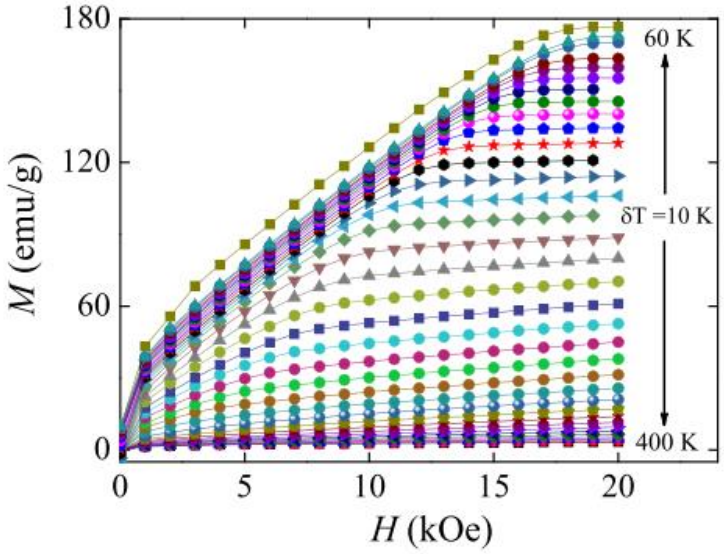

Figure 3. 11 *:* Magnetic isotherms of the studied Gd-Co based multilayer studied as a function of the applied magnetic field from 0 to 20 kOe with sweeping rate of 250 Oe/s

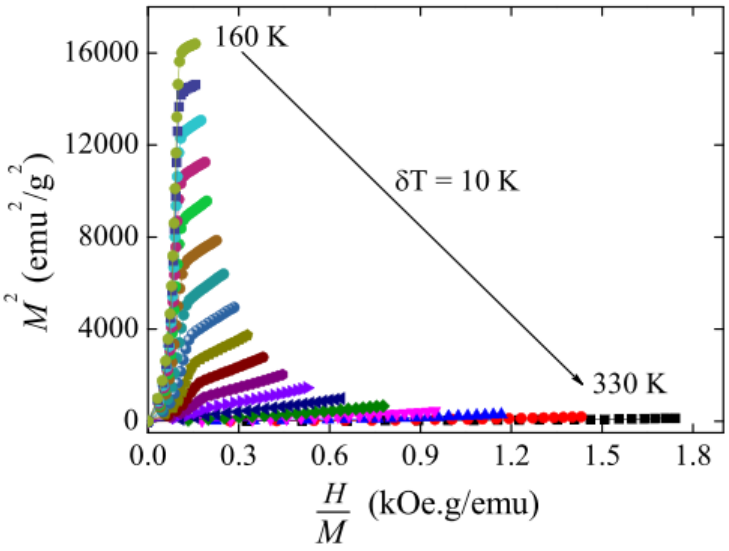

Figure 3. 12 *:* Arrott plots showing the evolution of M^2 as a function of $\frac{H}{M}$ for the studied Gd-Co based multilayer and for different values of temperature T.

Furthermore, we compared the values of $-\Delta S_M$ obtained for the studied Gd-Co alloy based multilayer stack with those obtained for a single 100 nm-thick Gd layer and for 100 nm-thick $Gd_{1-x}Co_x$ alloy layer with x = 0.44, 0.48, 0.52 and 0.56 (see figure 3.12). The values of $-\Delta S_M$ are obtained from the field dependence of the magnetization using the Maxwell relation

$$\Delta S_M(T, H_0) = \mu_0 \sum_i \frac{M_{i+1}(T_{i+1}, H) - M_i(T_i, H)}{T_{i+1} - T_i} \qquad (3.7)$$

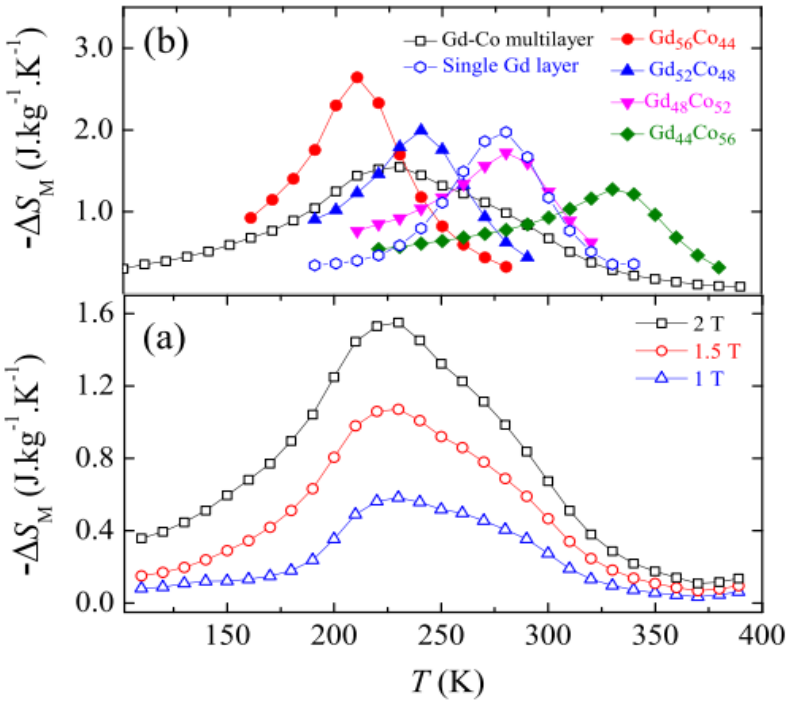

Figure 3. 13 *: Temperature dependence of the magnetic entropy change -ΔS_M* ***(a)*** *for the studied Gd-Co based multilayer while sweeping the magnetic field from 0 to H_{max} with H_{max}= 10 kOe, 15 kOe and 20 kOe,* ***(b)*** *for the studied Gd-Co multilayer, a 100 nm-thick Gd layer, and four 100 nm-thick $Gd_{100-x}Co_x$ single alloy layers with x = 44, 48, 52 and 56.*

The value of $-\Delta S_M$ I lower for the studied multilayer compared to the single Gd layer as well as the single Gd-Co alloy layers. However, the peak is much broader than for any of the single alloy layers. Note that the magnetic entropy is changed is not the only parameter to characterize

the potential of a magnetic refrigerant. Indeed, the relative cooling power can also prove important. The RCP quantifies the amount of heat that can be transferred between the hot and the cold ends. For the point of view of application, a large RCP over a wide temperature range coupled with a substantial MCE is desirable. The value of RCP can be calculated as

$$\mathrm{RCP}=-\Delta S_M \times \delta \mathrm{T}_{\mathrm{FWHM}} \quad (3.8)$$

With δT_{FWHM} is the full width at half maximum and $-\Delta \mathrm{S_M}$ is the maximum of magnetic entropy change [133].

From a technological point of view, it is important to obtain a large magnetic entropy change and a high RCP for a moderate magnetic field of 20 kOe. The measured RCP value for the Gd-Co alloys-based multilayer stack is 200 J/Kg. This RCP value is slightly smaller than that reported for $Gd_5Si_2Ge_2$ [123]. FeRh polycrystalline alloy [134]. Epitaxial MnAs [135], and $Gd_{48}Co_{52}$ amorphous ribbons [103] for the same magnetic field change of 20 kOe. At the same time, the measured RCP value for the studied Gd-Co based multilayer is higher than that observed in manganite thin films, such as $La_{0.67}Sr_{0.33}MnO_3$ [137], $La_{0.67}Ba_{0.33}Ti_{0.02}Mn_{0.98}O_3$ [138], or $La_{0.7}Sr_{0.3}MnO_3$ on $SrRuO_3$ super-lattices [139], Gd/W multilayered films [140], and $Gd_{62}Co_{38}$ amorphous ribbons [141]. We summarize in Table I the main performance related to the MCE of the above-presented materials as well as some others reported in the literature.

Materials	T_c (K)	$-\Delta S_M^{peak}(J/kg.K)$ $\Delta H = 20kOe$	$RCP(J/kg)$ $\Delta H = 20kOe$	ΔH (T)	References
Gd/W (40 nm)	275	1.41	52	1	[140]
$Gd_5Si_{2.7}Ge_{1.3}$ (788 nm)	190	3.7	75	2	[130]
Gd (30 nm)	285	1.6	70	1	[141]
MnAs (70 nm)	300	4	125	2	[143]
$La_{0.67}Sr_{0.44}MnO_3$ (31 nm)	70	0.3	10	1	[144]
$La_{0.67}Ba_{0.33}Ti_{0.02}Mn_{0.98}O_2$ (95 nm)	286	0.99	49	1	[138]
Ni-Mn-Ga (400 nm)	346	1.7	----	1	[145]
$[La_{0.67}Sr_{0.33}MnO_3/SrTiO_3]$ (20 nm)	321	1.1	15	1	[137]
$[La_{0.7}Sr_{0.30}MnO_3/SrRuO_3]$ (8 nm)	325	2.35	125	2	[139]
$Gd_{62}Co_{38}$ amorphous ribbons	193	2.8	81.4	1	[141]
$(Gd_{44}Co_{56})/(Gd_{48}Co_{52})/Gd_{52}Co_{48})/(Gd_{56}Co_{44})$ (100 nm)	230	1.54	200	2	This thesis

Table 3. 2*:* Overview of the main performances related to the magnetocaloric effect for the studied Gd-Co alloy-based multilayer stack and for other materials reported from the literature [130,137-145]

3.2.4 Conclusion

In summary, we have engineered a Gd-Co based multilayer stack sample to enhanced magnetocaloric properties. We have verified that the multilayer undergoes a second-order transition at the Curie temperature. The value of $-\Delta S_M$ and RCP for the studied Gd-Co alloy-based multilayer is compared to the one obtained for single Gd-Co alloy layers. The maximum $-\Delta S_M$ for the multilayer reach 1.54 $J.Kg^{-1}.K^{-1}$ for a magnetic field change from 0 to 20 kOe which is lower than for any of the single Gd-Co alloy layer. However, the $-\Delta S_M$ peak is much broader for the multilayer and the RCP value can reach 200 J/Kg. Such enhancement of the RCP demonstrates the potential of Gd-Co based multilayer for magnetic refrigeration application.

Chapter 4:

Tunable magneto-caloric effect in $Gd_{100-x}Tb_x$ heterostructures thin film

4.1 Introduction

The possibility of using magnetic refrigeration has become more reliable during the last twenty years, which will enable it to replace conventional refrigeration systems [149,150]. Such a change is desirable due to the advantages of using the magnetocaloric effect (MCE) for magnetic refrigeration application [151–153], thus leading to high refrigeration efficiency, small volume requirement, low cost, environmental friendliness, no noise pollution and better performance [154–156]. An excellent magnetic refrigerant should have large magnetic entropy change (ΔS_M) induced by low magnetic field change. According to the Curie–Weiss law for ferromagnetism, large magnetic entropy change ΔS_M (T,H) is expected at the Curie temperature (T_c) and for materials with larger values of effective magnetic moment. When a magnetic field is applied adiabatically to a magnetic material, the unpaired spins are aligned parallel to the field. The magnetic entropy of the material is lowered and the sample warms recovering the lost magnetic entropy through the increase of its lattice entropy. On the other hand, when the field is removed from the magnetic sample, the spin tends to randomize, increasing the magnetic entropy and lowering the lattice entropy and the temperature of the material [157–159]. MCE has mainly been investigated for bulk crystal and polycrystal materials [156,160,161]. However, a few studies have concentrated on thin films to investigate the role of size on the MCE. For instance, recent studies have shown that nanostructured Gd has a different magnetocaloric behavior when compared with the bulk counterparts [162,163]. The origin of this change appears to be a combination of interface defects and lower size effects. Moreover, an experimental investigation by Miller et al. based on magnetocaloric behavior of nanostructured Gd was done to carry diapers and Gd heterostructures [164]. The results showed that the maximum entropy is increased in Gd/W multilayer relative to the bulk state [164,165]. With the exception of gadolinium, all other rare earth metals have transition temperatures below ambient, more generally below 230 K. However, many applications concern the vicinity of ambient temperature. The use of these elements as refrigerants in this temperature range is therefore impossible. On the other hand, these materials can be used as substitutes for gadolinium in order to lower its Curie temperature and thus cover a wide temperature range.

In order to widen the range of refrigeration, we have chosen to study in this chapter the effect of terbium substitution of gadolinium on the magnetic properties, and magnetocaloric. Next, we will study a multilayer made of different [Gd/Tb] in order to investigate how magnetocaloric effect can be tuned using nanoscale material.

4.2 Fabrication and Measurements

The samples were grown at room temperature on (100)-silicon substrates using sputtering deposition with a base-pressure lower than 10-7 Torr. The Gd and Tb layers were deposited at room temperature (RT). A 3nm-Ta buffer layer was used as well as a 3nm-Ta capping layer to avoid oxidation of the rare-earth elements. The total magnetic thickness of the samples is kept constant and equal to 100 nm to ease the comparison of the magnetocaloric values. Two sets of samples were deposited: a series of ($Gd_{100-x}Tb_x$) samples with x (the atomic ratio) varying from 0 to 100; and a series of multilayers with a given ($Gd_{80}Tb_{20}$) equivalent composition and an increasing segregation of the Gd and Tb elements in regular alternating layers The samples are depicted schematically in Figure. 4.1.

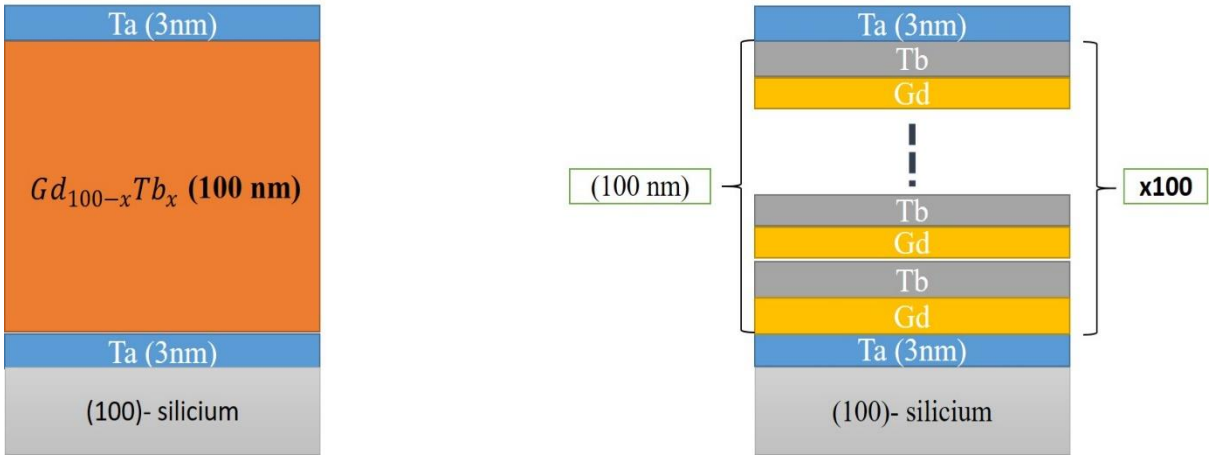

Figure 4. 1: Schematic of the two growth samples under investigation. The $Gd_{100-x}Tb_x$ alloy sample was grown with the Gd and Tb simultaneously deposited (left). The $[Gd/Tb]_{100}$ multilayer (right) has discrete layers containing Gd and Tb. This layer sequence is repeated 100 times. The total thickness of each sample is 100 nm.

4.3 Structural characterization

In order to verify the hexagonal structure, X-ray diffraction measurement was carried out. The X-ray diffraction spectra of the selected $Gd_{40}Tb_{60}$ and $Gd_{80}Tb_{20}$ sample (Figure 4.2) shows that the obtained diffraction peak correspond to the hexagonal, close-packed structure (N° 89-2934). The $Gd_{100-x}Tb_x$ sample displayed several relatively strong and well-defined reflection peaks in the 2θ region of 30- 70°, and the position and relative intensities of all detectable peaks matched well with those from the standard JCPDS patterns (as shown in Figure 4.2) indicating that the resulting materials has a hexagonal, close-packed structure. Traces of any other phases, kind of detectable impurities or intermediate phase were not observed. The diffraction peaks corresponding to the (002), (101) and (004) reflections provided clear evidence for hexagonal, close-packed structure, confirming the crystallization of the $Gd_{100-x}Tb_x$ alloy thin film.

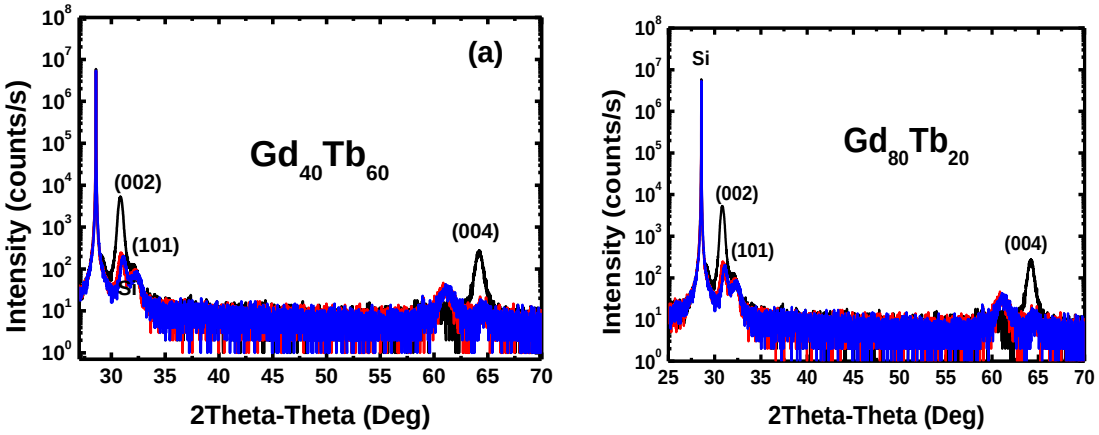

Figure 4. 2*:*X-ray diffractograms for selected samples. (a) $Gd_{40}Tb_{60}$ (b) $Gd_{80}Tb_{20}$

4.4 Magnetic and magnetocaloric properties

Magnetic properties of the films were carried out using a Quantum Design Physical Property Measurement System with a vibrating sample magnetometer attachment. Isothermal magnetization (*M–H*) curves were measured in persistent mode using a 100 Oe/s sweep rate and a 5 s averaging time using a vibrating sample magnetometer. The temperatures used ranged from 225 to 350K, in 10 or 5K increments. The magnetization data were normalized to the nominal $Gd_{100-x}Tb_x$ area of each sample.

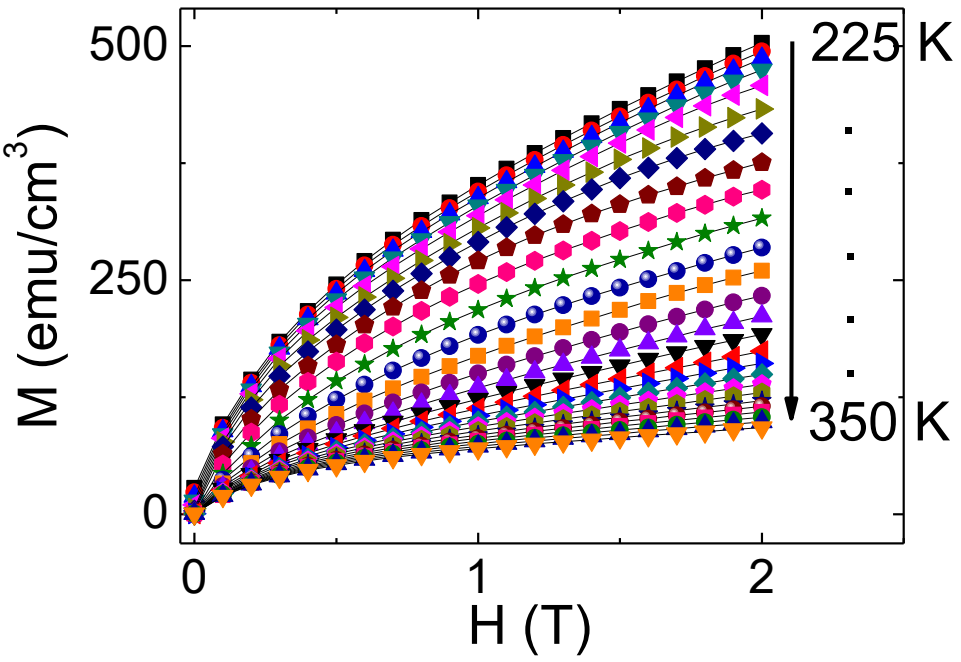

Figure 4. 3*:* Magnetic isotherms of a $Gd_{80}Tb_{20}$ alloy compound measured at several temperatures around TC in a magnetic field applied out-of-plane.

Figure 4.3 illustrates the type of measurements that have been performed on a typical ($Gd_{80}Tb_{20}$) alloy sample. We observe that the maximum variation of magnetization is occurring at the Curie temperature (T_C = 270 K) where the material is subject to a second-order transition between its ferromagnetic and paramagnetic state.

The corresponding curve of the entropy variation can then be drawn as seen on figure 4.4. The modification of the T_C can directly be tracked following the drift of the maximum variation of entropy as the Tb concentration increases. The decrease in the transition temperature with increasing concentration of terbium is due to the fact that the Curie temperature of Tb (222 K) [166,167] is lower than that of Gd (294 K) [160]. Thus, doping of Gd with Tb decreases the exchange interactions which cause the reduction of T_c. However, it has already been demonstrated that in bulk sample, substituting the gadolinium with 50% of terbium decreases the Curie temperature from 294 K to 264 K without affecting the magnetocaloric properties of the material [168].

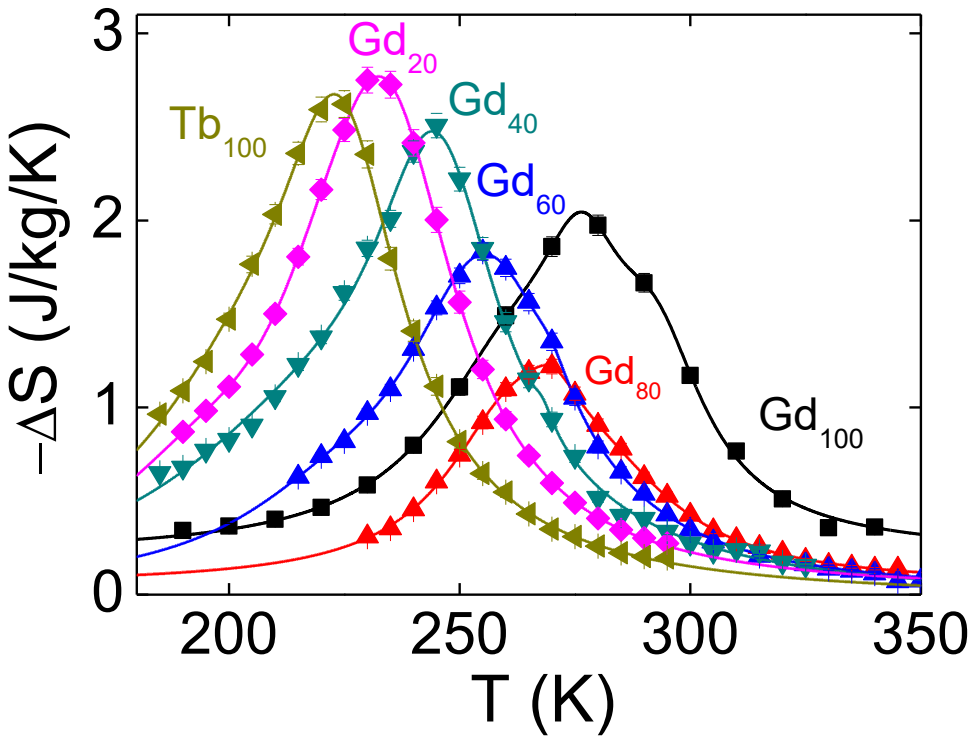

Figure 4. 4*:* Temperature dependence of magnetic entropy change in Gd100-xTbx alloys compounds in a field of 2 T. Lines are just guides to the eyes.

Thus substituting Gd with Tb, we can cover a range of refrigeration between 260 and 300 K (-13 and 25°C). In addition, the active magnetic regenerative refrigeration (AMRR) requires a strong magnetocaloric material power over a wide temperature range. In the case of systems

that use the Ericsson cycle as a refrigeration cycle, the change in total entropy of the refrigerant must be as constant as possible over the relevant temperature range which is not the case for the $Gd_{100-x}Tb_x$ bulk alloys [168].

Even if the position of the peak is easily controlled by the ratio between the two elements, the amplitude of the peak and the relative cooling power (RCP) coefficient associated to the area under the curve evolve differently and are strongly varying depending on the composition. Indeed, the amplitude of the peak increases with the Tb content, and is attributed to the increase of the magnetic moment of the $Gd_{100-x}Tb_x$ film upon alloying with the Tb element [169]. Moreover, for x = 20, 40 and 60%, the RCP is lower than for pure Gd, while for x = 80% the properties are enhanced compared to pure Gd.

To study the effect of interface and low dimension on the MCE, we compare the magnetocaloric behavior of Gd-Tb compouds with the same thickness and net concentration but with a different atomic ordering, namely Gd-Tb alloys and multilayers. We started with the concentration giving an entropy peak close to RT: $Gd_{80}Tb_{20}$ (100 nm). Then, we grew multilayers with the same atomic composition, but containing a segregation between the Gd and Tb atoms. Figure 4.4 show that the peak of entropy variation is evolving between a single peak when the [Gd/Tb] multilayer is very similar to an alloy (100 and 50 layers) (Figure 4.5(a)–(c)), to a double peak when the two elements are more spatially separated (10 and 2 layers) (Figure 4.5(d)–(e)). Indeed, the position of the two peaks matches with those of the pure Tb and Gd elements and their associated T_c, as depicted in Figure 4.5(f). Moreover, the studied [Gd/Tb] multilayers show a much broader entropy peak than for the corresponding alloy, reaching a value of approximately 50 K. Furthermore, a higher number of layers (100 and 50 layers) strengthens the exchange interaction between the two rare-earth elements. This exchange ends up in an interaction between neighbors very similar to the one of an alloy.

However, we can see on the figure 4.6 that the RCP is much higher than for the corresponding alloy. In our case, we define the RCP as followed:

$$\mathrm{RCP} = -\Delta S_M \times \delta T_{FWHM} \quad (4.1)$$

where T_1 and T_2 are the temperatures corresponding to the limits of the FWHM of the entropy variation peak.

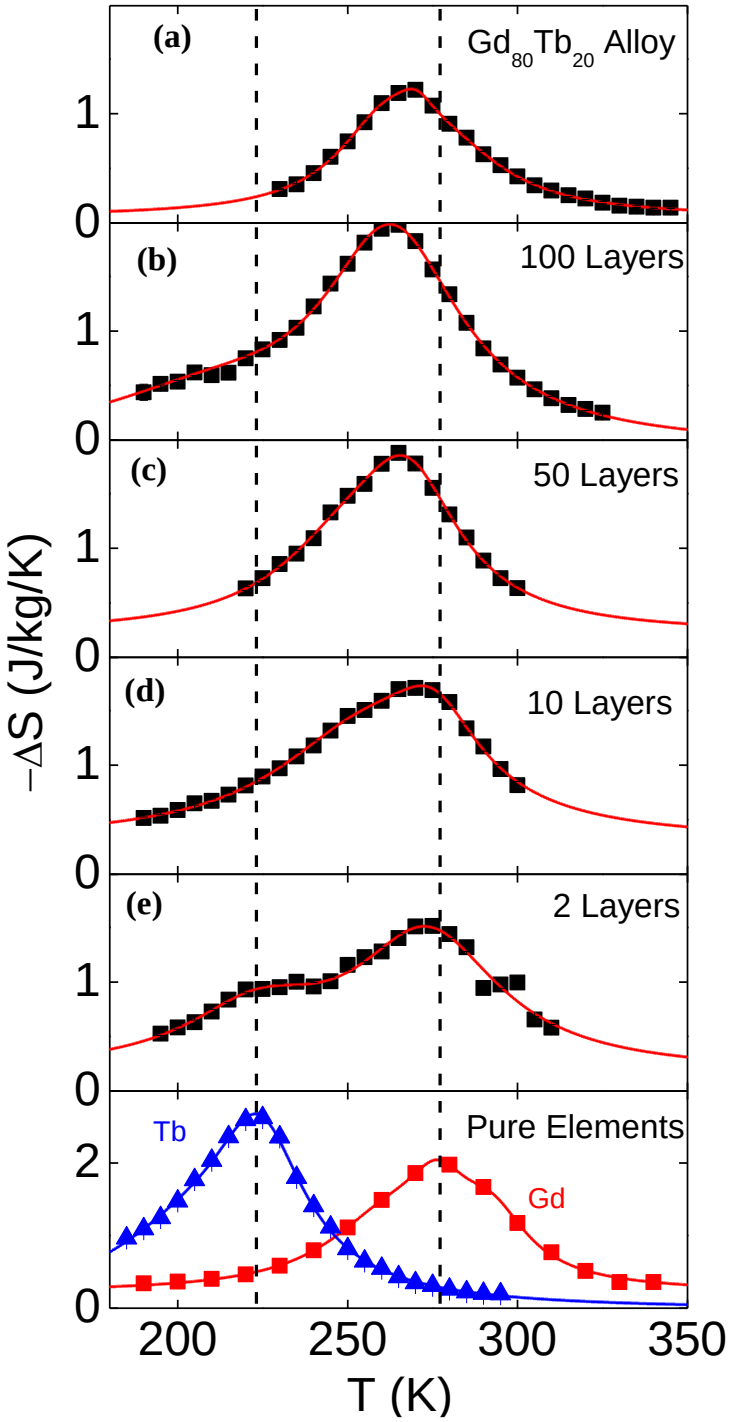

Figure 4. 5*:* Temperature dependence of magnetic entropy change in pure Gd and Tb, [Gd/Tb] alloy and multilayers with an ($Gd_{80}Tb_{20}$) equivalent composition in a field of 2 T.

The dashed lines indicated the maximum entropy change for pure elements. Lines are just guides to the eyes.

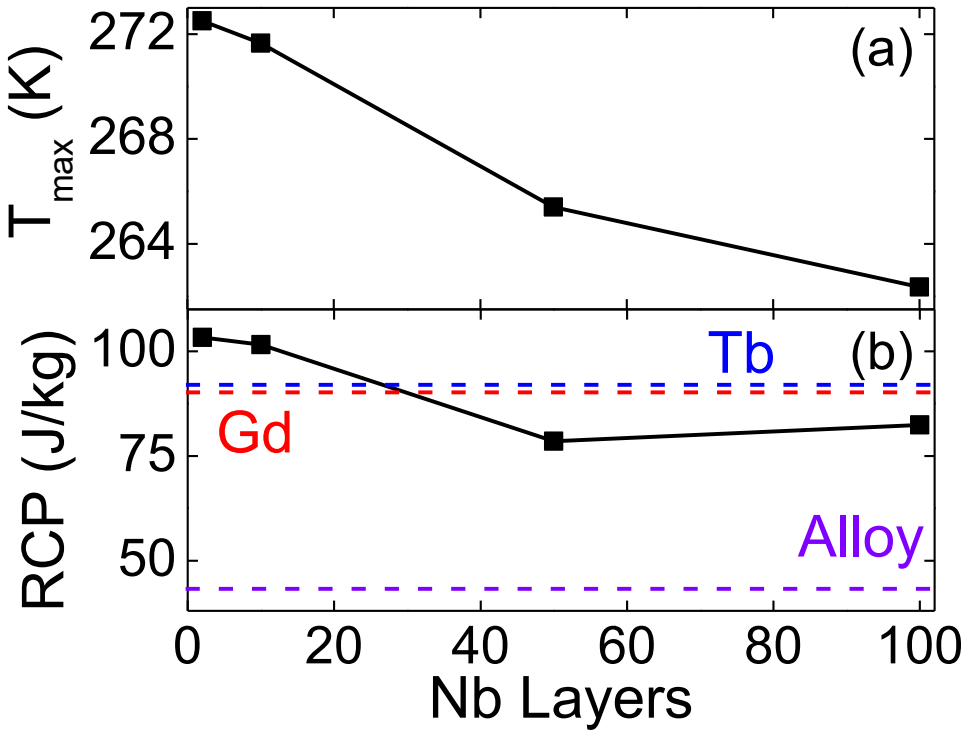

Figure 4. 6*:* (a) Position of the maximum variation of entropy for $Gd_{80}Tb_{20}$ multilayers with different number of layers. (b) The respective RCP values calculated for this multilayer. The purple dashed line represents the value of an alloy sample with an equivalent composition, while the red and blue dashed lines indicates the values for a sample of pure Tb or Gd.

Whatever the number of layers, the RCP is almost twice as big as the one from the corresponding $Gd_{80}Tb_{20}$ alloy for an equal thickness of the film. Furthermore, the temperature at which the maximum entropy is obtained is not changing much, and is very close to the one of a pure Gd film. This finding is probably due to the unbalance between the two elements (80% of Gd in this example). Therefore, the ordering of the atoms seems to play a key effect in the MCE, which is in agreement with previous study [168,170]. This finding had also been seen in the case of annealed samples where the properties are enhanced, thanks to a better

crystallinity [171]. These results suggest that a multilayer stacking could greatly improve the magnetocaloric properties in the Gd-Tb system without requiring the introduction of additional elements. From the comparison with Gd data as well as from the technological point of view, our results underline that our matrial can be used in cooling system based on the magnetic refrigeration.

4.5 Summary

As a conclusion we demonstrated the possibility to independently tune the position and amplitude of the peak of entropy variation in $Gd_{1-x}Tb_x$ systems. Even if a reduction of the of the magnetocaloric properties through a diminution of the RCP is observed in mere thin films alloys, a recovery is possible by creating a multilayer structure. Thanks to this approach the variation of entropy can be controlled continuously from the individual properties of its constituting elements. This study opens up new possibilities in the control and optimization of the magnetocaloric effect in magnetic thin films.

General conclusions and perspectives

In this final chapter, the most important achievements described throughout this thesis will be summarized. The results answering the questions formulated in the general introduction chapter will be remarked, and new questions opening future work paths will be stated. At the end, the perspectives for future work will be indicated.

Magnetic and magnetocaloric studies on Gd thin films and Gd alloy thin films have emphasized the important roles of reduced dimensionality in magnetic refrigerant materials which are key components in advanced magnetic coolers. The major findings of the thesis research are summarized below:

The first part of this thesis, thin films of $Gd_{100-x}Co_x$ alloy compounds were deposited on silicon substrate using sputtering techniques. The magnetic and magneto-caloric effect of $Gd_{100-x}Co_x$ (x=44, 48, 52, 56) thin films were investigated. The Curie temperature increase when the concentration of Cobalt element increases. The maximal magnetic entropy changes of the samples reached a maximum at the Curie temperature. Under an applied magnetic field of 2 T, the value of magnetic entropy changes is found to be 2.64 for x = 44, respectively. Moreover, the samples present an important relative cooling power "RCP" higher than 140 J/Kg which considered as a recommended parameter for a wide temperature range in magnetic refrigeration application. Moreover, critical properties study on the second-order ferromagnetic transition of $Gd_{100-x}Co_x$ thin film demonstrate that the magnetic interaction around T_c can be described with the mean field model corresponding to long-range interaction.

In this context, we have demonstrated an effective approach for improving the magnetocaloric properties of Gd-Co based multilayer. We have verified that the multilayer undergoes a second-order transition at the Curie temperature. The value of $-\Delta S_M$ and RCP for the studied Gd-Co alloy-based multilayer is compared to the one obtained for single Gd-Co

alloy layers. The maximum $-\Delta S_M$ for the multilayer reach 1.54 $J.Kg^{-1}.K^{-1}$ for a magnetic field change from 0 to 20 kOe which is lower than for any of the single Gd-Co alloy layer. However, the $-\Delta S_M$ peak is much broader for the multilayer and the RCP value can reach 200 J/Kg. Such enhancement of the RCP demonstrates the potential of Gd-Co based multilayer for magnetic refrigeration application.

Finally, we demonstrated the possibility to independently tune the position and amplitude of the peak of entropy variation in Gd-Tb systems. The ordering temperature and magnetic entropy changes of $Gd_{100-x}Tb_x$ alloy thin films could be tuned by changing the alloy's composition. Moreover, we demonstrate that creating [Gd/Tb] multilayers with the same thickness and concentration of the studied $Gd_{100-x}Tb_x$ alloy films enables to strongly increase the relative cooling power, and reach values twice as big as from the corresponding alloys. Thanks to this approach, the variation of entropy can be controlled continuously from the individual properties of its constituting elements. This study opens up new possibilities in the control and optimization of the magnetocaloric effect in magnetic thin films.

Future Research

Further improvement in the *RC* of Gd thin films is essential in driving them into their real-world microscale solid-cooling applications. One possible approach is to create multi-layer films that possess Gd layers mediated by soft ferromagnetic layers such as FeNi. Magnetic coupling between the different ferromagnetic layers at their interfaces can be tuned to improve the magnetocaloric responses of the films.

Gd-based alloys in the form of thin film are ideal for a variety of magnetic micro-cooling applications. Their MCE and *RC* can be further improved by engineered with soft ferromagnetic layers such as FeNi, creating multi-layer structures. Combing the molecular beam epitaxy and sputtering technique is most appropriate for making these novel multi-layers thin film.

Combined theoretical and experimental studies will be needed to validate the above hypotheses. Bringing these fundamental studies to the point of making prototype refrigeration devices will require the concerted effort of interdisciplinary scientists and engineers.

Reference

[1] Khovaylo, V.V.; Rodionova, V.V.; Shevyrtalov, S.N.; and Novosad, V. Magnetocaloric effect in reduced dimensions: Thin films, ribbons, and microwires of Heusler alloys and related compounds. Phys. Status Solidi B 2014, 251, 2104-2113.

[2] Miller, C.W.; Belyea, D.D.; Kirby, B.J. Magnetocaloric effect in nanoscale thin films and heterostructures. J. Vac. Sci. Technol. 2014, 32, 040802.

[3] D. T. Morelli, A. M. Mance, J. V. Mantese, and A. L. Micheli, J. Appl. Phys. 79, 373 (1996).

[4] P. Lampen, N.S. Bingham, M.H. Phan, H.T. Yi , S.W. Cheong, and H. Srikanth, Phys. Rev. B 89, 144414 (2014)

[5] X. Moya et al., Nat. Mater. 12, 52 (2013)

[6] A. A. Fraerman, I. A. Shereshevskii, JETP Letters **101**, 618 (2015)

[7] V. Mello, A. L. Dantas, and A. Carric¸o, Solid State Commun. 140, 447 (2006).

[8] D. D. Belyea, T. S. Santos, and C. W. Miller, Magnetocaloric effect in epitaxial $La_{0.56}Sr_{0.44}MnO_3$ Alloy and digital heterostructures J. Appl. Phys. **111**, 07A935 (2012)

[9] Ravi L. Hadimani, J. H. B. Silva, A. M. Pereira, D. L. Schlagel, T. A. Lograsso, Y. Ren, X.
Zhang, David C. Jiles, and J. P. Araujo, Appl. Phys. Lett. **106**, 032402 (2015)

[10] T. Christiaanse and E. Brück, Metall. Mater. Trans. E, vol. 1, p. 36, 2014.

[11] P. Weiss and A. Piccard, J. Phys. (Paris), vol. 7, p. 103, 1917.

[12] P. Weiss and A. Piccard, Comptes Rendus, vol. 166, p. 352, 1918.

[13] E. Warburg, Ann. Phys., vol. 249, p. 141, 1881

[14] A. Smith, C. Bahl, R. Bjork, K. Engelbrecht, K. Nielsen and N. Pryds, Adv. Energy Mater., vol. 2, p. 1288, 2012.

[15] P. Debye, Ann. Physik., vol. 81, p. 1154, 1926.

[16] W. Giauque, J. Amer. Chem. Soc., vol. 49, p. 1864, 1927.

[17] W. Giauque and D. MacDougall, Phy. Rev., vol. 43, p. 768, 1933.

[18] G.V. Brown, J. Appl. Phys., vol. 47, p. 3673, 1976.

[19] J. Barclay, in Proceeding of the Second Biennial on Refrigeration for Cryocooler Sensors and Electronic Systems, 1983.

[20] V. Pecharsky and K. Gschneidner, J. Magn. Magn. Mater., vol. 200, p. 44, 1999.

[21] V. K. Pecharsky and K. A. Gschneider Jr., Phys. Rev. Lett., vol. 78, p. 4494, 1997.

[22] C. Zimm, A. Jastrab, A. Sternberg, V. Pecharsky, K. Gschneider Jr., M. Osborne and I. Anderson, Adv. Cryog. Eng., vol. 43, p. 1759, 1998.

[23] Cooling post, "Debut for magnetic refrigeration wine cooler," 2015. [Online]. Available: http://www.coolingpost.com/world-news/debut-for-magnetic-refrigeration-wine-cooler/. [Accessed 11 March 2016].

[24] E. Brück, H. Yibole and L. Zhang, Phil. Trans. R. Soc. A, vol. 374, 2016.

[25] A. Morrish, in The Physical Principles of Magnetism, New York, Wiley, 1965.

[26] J. Lyubina, "Magnetocaloric materials," in Novel functional magnetic materials, Springer, 2016, pp. 115-186.

[27] M.H. Phan, V. Franco, N.S. Bingham, H. Srikanth, and N.H. Hur, J. Alloys and Comp. **508**, 238 (2010)

[28] P. Zhang, T.L. Phan, and S.C. Yu, T. D. Thanh, N. H. Dan, V. D. Lam, P. Lampen, H. Srikanth, and M.H. Phan, J. Magn. Magn. Mater. 348,146 (2013)

[29] P. Lampen, M.H. Phan,K. Kovnir, P. Chai, M. Shatruk, and H. Srikanth, Phys. Rev. B 90, 174404 (2014)

[30] M. H. Phan, G.T. Woods, A. Chaturvedi, S. Stefanoski, G.S. Nolas, and H. Srikanth, Appl. Phys. Lett. 93, 252505 (2008)

[31] H. E. Stanley, Introduction to phase transitions and critical phenomena (Oxford University Press, London, 1971)

[32] B. Widom, The Journal of Chemical Physics 41, 1633 (1964)

[33] J. S. Kouvel and M. E. Fisher, Phys. Rev. 136, A1626-A1632 (1964)

[34] A. Arrott and J. Noakes, Phys. Rev. Lett. 19, 786 (1967)

[35] M.H. Phan, J. Gass, N. A. Frey, H. Srikanth, M. Angst, B.C. Sales, and D. Mandrus, Solid State Communications 150, 341 (2010)

[36] M.H. Phan, B. Morales, H. Srikanth, C.L. Zhang and S.W. Cheong, Phys. Rev. B 81, 09441 (2010)

[37] P. Lampen, N.S. Bingham, M.H. Phan, H.T. Yi , S.W. Cheong, and H. Srikanth, Phys. Rev. B 89, 144414 (2014)

[38] V. Franco, J.S. Blázquez, B. Ingale, and A. Conde, Annu. Rev. Mater. Res. 42, 305 (2012)

[39] N. A. de Oliveira and P. J. von Ranke, Physics Reports 489, 89 (2010)

[40] K.A. Gschneidner jr, V.K. Pecharsky, Annu. Rev. Mater. Sci. 30, 387 (2000)

[41] N. A. de Oliveira and P. J. von Ranke, Physics Reports 489, 89 (2010)

[42] N.S. Bingham, M.H. Phan, H. Srikanth, M.A. Torija, and C. Leighton, J. Appl. Phys. 106, 023909 (2009)

[43] "Low Dimensionality Effects in Complex Magnetic Oxides," - Paula J. Lampen-Kelley, PhD thesis, University of South Florida, 2015. http://gradworks.umi.com/37/00/3700295.html

[44] V. Franco, J.S. Blazquez, A. Conde, Appl. Phys. Lett. **89**, 222512 (2006).

[45] CM Bonilla, J Herrero-Albillos, F Bartolomé, LM García, Phys. Rev. B **81**, 224424 (2010)

[46] M.H. Phan, V. Franco, A. Chaturvedi, S. Stefanoski, G.S. Nolas, and H. Srikanth, Phys. Rev. B **84**, 054436 (2011)

[47] V. Franco and A. Conde, Scr. Mater. 67, 594 (2012)

[48] H. Ucar, J. Ipus, V. Franco, M. McHenry, and D. Laughlin, JOM 64, 782 (2012).

[49] K. G. Sandeman, Scr. Mater. 67, 566 (2012).

[50] D. T. Morelli, A. M. Mance, J. V. Mantese, and A. L. Micheli, J. Appl. Phys. 79, 373 (1996).

[51] V. Mello, A. L. Dantas, and A. Carric¸o, Solid State Commun. 140, 447 (2006).

[52] F. C. M. Filho, V. D. Mello, A. L. Dantas, F. H. S. Sales, and A. S. Carric¸o, J. Appl. Phys. 109, 07A914 (2011).

[53] M. H. Phan, M. B. Morales, C. N. Chinnasamy, B. Latha, V. G. Harris, and H. Srikanth, J. Phys. D 42, 115007 (2009).

[54] T. Jiang, L. Xie, Y. Yao, Y. Liu, and X. Li, Mater. Lett. 76, 25 (2012).

[55] T. Mukherjee, S. Sahoo, R. Skomski, D. J. Sellmyer, and C. Binek, Phys. Rev. B 79, 144406 (2009).

[56] Z. Wei, A. Chak-Tong, and D. You-Wei, Chin. Phys. B 22, 057501 (2013).

[57] J. C. Debnath, J. H. Kim, Y. Heo, A. M. Strydom, and S. X. Dou, J. Appl. Phys. 113, 063508 (2013).

[58] Q. Zhang, S. Thota, F. Guillou, P. Padhan, V. Hardy, A. Wahl, and W. Prellier, J. Phys. Condens. Matter 23, 052201 (2011).

[59] T. S. Santos, S. J. May, J. L. Robertson, and A. Bhattacharya, Phys. Rev. B 80, 155114 (2009).

[60] V. S. Kumar, R. Chukka, Z. Chen, P. Yang, and L. Chen, AIP Adv. 3, 052127 (2013).

[61] S. Maat, J.-U. Thiele, and E. E. Fullerton, Phys. Rev. B 72, 214432 (2005).

[62] X. Moya et al., Nat. Mater. 12, 52 (2013)

[63] C. Binek and V. Burobina, Appl. Phys. Lett. 102, 031915 (2013).

[64] P. Lampen, N. S. Bingham, M. H. Phan, H. Kim, M. Osofsky, A. Pique, T. L. Phan, S. C. Yu, and H. Srikanth, Appl. Phys. Lett. 102, 062414 (2013).

[66] C. Thiele, K. D€orr, O. Bilani, J. R€odel, and L. Schultz, Phys. Rev. B 75, 054408 (2007).

[67] J. Marcos, A. Planes, L. Ma~nosa, F. Casanova, X. Batlle, A. Labarta, and B. Martinez, Phys. Rev. B 66, 224413 (2002).

[68] W. Dun-Hui, H. Zhi-Da, X. Hai-Cheng, M. Sheng-Can, C. Shui-Yuan, Z. Cheng-Liang, and D. You-Wei, Chin. Phys. B 22, 077506 (2013).

[69] O. Heczko, M. Thomas, R. Niemann, L. Schultz, and S. F€ahler, Appl. Phys. Lett. 94, 152513 (2009).

[70] N. A. de Oliveira and P. J. von Ranke, Phys. Rev. B 77, 214439 (2008).

[71] R. Niemann, O. Heczko, L. Schultz, and S. F€ahler, Appl. Phys. Lett. 97, 222507 (2010).

[72] Y. Zhang, R. A. Hughes, J. F. Britten, P. A. Dube, J. S. Preston, G. A. Botton, and M. Niewczas, J. Appl. Phys. 110, 013910 (2011).

[73] V. Recarte, J. I. Perez-Landazabal, V. Sanchez-Alarcos, V. A. Chernenko, and M. Ohtsuka, Appl. Phys. Lett. 95, 141908 (2009).

[74] P. F. Xu, S. H. Nie, K. K. Meng, S. L. Wang, L. Chen, and J. H. Zhao, Appl. Phys. Lett. 97, 042502 (2010).

[75] D. D. Dung, D. A. Tuan, D. V. Thiet, Y. Shin, and S. Cho, J. Appl. Phys. 111, 07C310 (2012).

[76] S. Gama, A. A. Coelho, A. de Campos, A. M. G. Carvalho, F. C. G. Gandra, P. J. von Ranke, and N. A. de Oliveira, Phys. Rev. Lett. 93, 237202 (2004).

[77] D. H. Mosca, F. Vidal, and V. H. Etgens, Phys. Rev. Lett. 101, 125503 (2008).

[78] J.-Y. Duquesne, J.-Y. Prieur, J. A. Canalejo, V. H. Etgens, M. Eddrief, A. L. Ferreira, and M. Marangolo, Phys. Rev. B 86, 035207 (2012).

[79] EL HADRI, Mohammed Salah. Magnetization reversal mechanism leading to all-optical helicity-dependent switching. 2016. Thèse de doctorat.R.E. Maringer, C.E. Mobley, J. Vac. Sci. Technol. **11**, 1067 (1974)

[80] Rigaku, Powder diffraction optics for SmartLab X-ray diffractometer, Rigaku J. 26 (2) (2010) 29–30.

[81] Foner, Simon. "Versatile and sensitive vibrating-sample magnetometer." Review of Scientific Instruments **30** ,548-557 (1959).

[82] Gschneidner Jr., K.A.; Pecharsky, V.K. Thirty years of near room temperature magnetic cooling: Where we are today and future prospects. Int. J. Refrig. 2008, 31, 945-961.

[83] Fujita, A.; Yako, H. Stability of metallic, magnetic and electronic states in NaZn13-type La(Fe*x*Si1−*x*)13 magnetocaloric compounds. Scr. Mater. 2012, 67, 578-583.

[84] Liu, E.K; Wang, W.H.; Lin, F.; Zhu, W.; Li, G.J.; Chen, J.L.; Zhang, H.W.; Wu, G.H.; Jiang, C.B.; Xu, H.B.; de Boer, F. Stable magnetostructural coupling with tunable magnetoresponsive effects in hexagonal ferromagnets. Nat. Commun. 2012, 3, 873.

[85] Trung, N.T.; Zhang, L.; Caron, L.; Buschow, K.H.J.; Brück, E. Giant magnetocaloric effects by tailoring the phase transitions. Appl. Phys. Lett. 2010, 96, 172504.

[86] Gschneidner Jr., K.A., Pecharsky, V.K.; Tsokol, A.O. Recent developments in magnetocaloric materials. Rep. Prog. Phys. 2005, 68, 1479–1539.

[87] Pecharsky, V.K.; Gschneidner Jr., K.A. Giant Magnetocaloric Effect in Gd5(Si2Ge2). Phys. Rev. Lett. 1997, 78, 4494.

[88] Wada, H.; Tanabe, Y. Giant magnetocaloric effect of MnAs1−xSbx. Appl. Phys. Lett. 2001, 79, 3302.

[89] Hu, F.; Shen, B.; Sun, J.; Cheng, Z.; Rao, G.; Zhang, X. Influence of negative lattice expansion and metamagnetic transition on magnetic entropy change in the compound LaFe11.4Si1.6. Appl. Phys. Lett. 2001. 78, 3675.

[90] Tegus, O.; Brück, E.; Buschow, K. H. J.; de Boer, F. R. Transition-metal-based magnetic refrigerants for room-temperature applications. Nature 2002, 415, 150–152.

[91] Krenke, T.; Duman, E.; Acet, M.; Wassermann, E.F.; Mañosa, L.; Planes, A. Inverse magnetocaloric effect in ferromagnetic Ni–Mn–Sn alloys. Nat. Mater. 2005, 4, 450–454.

[92] Miller, C.W.; Williams, D.V.; Bingham, N.S.; Srikanth, H. Magnetocaloric effect in Gd/W thin film heterostructures. J. Appl. Phys. 2010, 107, 09A903.

[93] Miller, C.W.; Belyea, D.D.; Kirby, B.J. Magnetocaloric effect in nanoscale thin films and heterostructures. J. Vac. Sci. Technol. 2014, 32, 040802.

[94] Zhang, Q.; Thota, S.; Guillou, F.; Padhan, P.; Hardy, V.; Wahl, A.; Prellier, W. Magnetocaloric effect and improved relative cooling power in (La0.7Sr0.3MnO3/SrRuO3) superlattices. J. Phys. Condens. Matter 2001, 23, 052201.

[95] Oumezzine, M.; Galca, A.-C. ; Pasuk, I.; Chirila, C.; Leca, A.; Kuncser, V.; Tanase, L.C.; Kumcser, A.; Ghica, C.; Oumezzine, M. Structural, magnetic and magnetocaloric effects in epitaxial La0.67Ba0.33Ti0.02Mn0.98O3 ferromagnetic thin films grown on 001-oriented SrTiO3 substrates. Dalt. Trans. 2016, 45, 15034-15040.

[96] Zhou, T.; Cher, M.K.; Shen, L.; Hu, J.F.; Yuan, Z.M. On the origin of giant magnetocaloric effect and thermal hysteresis in multifunctional α-FeRh thin films. Phys. Lett. A 2013, 377, 3052-3059.

[97] Recarte, V.; Pérez-Landazábal J. I.; Sánchez-Alárcos, V.; Chernenko, A.; Ohtsuka, M. Magnetocaloric effect linked to the martensitic transformation in sputter-deposited Ni–Mn–Ga thin films. Appl. Phys. Lett. 2009, 95, 141908.

[98] Mosca, D.H.; Vidal, F.; Etgens, V.H. Strain engineering of the magnetocaloric effect in MnAs epilayers. Phys. Rev. Lett. 2008, 101, 125503.

[99] Franco, V.; Blázquez, J.S.; Ingale, B.; Conde, A. The magnetocaloric effect and magnetic refrigeration near room temperature: Materials and models. Annu. Rev. Mater. Res. 2012, 42, 305-342.

[100] Gschneidner Jr., K.A.; Pecharsky, V.K. Magnetocaloric materials. Annu. Rev. Mater. Sci. 2000, 30, 387-429.

[101] Phan, M. H.; Yu, S.C. Review of the magnetocaloric effect in manganite materials. J. Magn. Magn. Mater. 2007, 308, 325-340.

[102] Lampen, P.; Bingham, N.S.; Phan, M.H.; Kim, H.; Osofsky, M.; Piqué, A.; Phan, T.L.; Yu, S.C.; Srikanth, H. Impact of reduced dimensionality on the magnetic and magnetocaloric response of La0.7Ca0.3MnO3. Appl. Phys. Lett. 2013, 102, 062414.

[103] Lampen-Kelley, P.J. Low dimensionality effects in complex magnetic oxides, Ph.D. Thesis, University of South Florida, Tampa, 2015.

[104] Khovaylo, V.V.; Rodionova, V.V.; Shevyrtalov, S.N.; and Novosad, V. Magnetocaloric effect in reduced dimensions: Thin films, ribbons, and microwires of Heusler alloys and related compounds. Phys. Status Solidi B 2014, 251, 2104-2113.

[105] Tadout, M.; Lambert, C.H.; El Hadri, M.S.; Mounkachi, O.; Benyoussef, A.; Hamedoun, M.; Benaissa, M.; Mangin, S. Engineered Gd-Co based multilayer stack to enhanced magneto-caloric effect and relative cooling power. J. Appl. Phys. 2018, 123, 053902.

[106] See Supplemental Material for XRD patterns of the studied Gd-Co alloy thin films.

[107] Hansen, P.; Clausen, C.; Much, G.; Rosenkranz, M.; Witter, K. Magnetic and magneto-optical properties of rare-earth transition-metal alloys containing Gd, Tb, Fe, Co. J. Appl. Phys. 1989, 66, 756.

[108] Inoue, J.; Shimizu, M. Volume dependence of the first-order transition temperature for RCo2 compound. J. Phys. F: Met. Phys. 1982, 12, 1811.

[109] Banerjee, B.K. On a generalised approach to first and second order magnetic transitions. Phys. Lett. 1964, 12, 16-17.

[110] Zhang, C.L.; Wang, D.H.; Han, Z.D.; Xuan, H.C.; Gu, B.X.; Du Y.W. Large magnetic entropy changes in Gd–Co amorphous ribbons. J. Appl. Phys. 2009, 105, 013912.

[111] Franco, V.; Blázquez, J.S.; Conde, A. Field dependence of the magnetocaloric effect in materials with a second order phase transition: A master curve for the magnetic entropy change. Appl. Phys. Lett. 2006, 89, 222512.

[112] Franco, V.; Caballero-Flores, R.; Condea, A.; Dong, Q.Y.; Zhang, H.W. The influence of a minority magnetic phase on the field dependence of the magnetocaloric effect. J. Magn. Magn. Mater. 2009, 321, 1115-1120.

[113] Widom, B. Equation of state in the neighborhood of the critical point. J. Chem. Phys. 1965, 43, 3898.

[114] Sahana, M.; Rössler, U.K.; Ghosh, N.; Elizabeth, S.; Bhat, H.L.; Dörr, K.; Eckert, D.; Wolf, M.; Müller, K.-H. Critical properties of the double-exchange ferromagnet Nd0.6Pb0.4MnO3. Phys. Rev. B 2003, 68, 144408.

[115] K. A. Gschneidner, Jr. and V. K. Pecharsky, Magnetic refrigeration materials J. Appl. Phys. **85**, 5365(1999).

[116] G. L. Liu, D. A. Zhao, H. Y. Bai, W. H. Wang, and M. X. Pan, Room temperature table-like magnetocaloric effect in amourphous $Gd_{50}Co_{45}Fe_5$ ribbon J. Phys. D: Appl. Phys. **49**, 055004(2016).

[117] GschneidnerJr, Karl A., V. K. Pecharsky, and A. O. Tsokol. Recent developments in magnetocaloric materials. Reports on progress in physics **68.6** 1479(2005).

[118] S. Dan'kov, A. M. Tishin, V. K. Pecharsky, and K. A. Gschneidner, Jr., Phys. Rev. B **57**, 3478 (1998).

[119] A. Y. Dong, B. G. Shen, J. Chen, J. Shen, H. W. Zhang, and J. R. Sun, J. Appl. Phys. **105**, 053908(2009).

[120] E. E. Bruck, O. Tegus, D. T. Cam Thanh, N. T. Trung, and K. H. J. Buschow, Int. J. Refrig. **31**, 763(2008).

[121] H. Wada and Y. Tanabe, Giant magnetocaloric effect of MnAs1-xSbx Appl. Phys. Lett **79**, 3302 (2001)

[122] V. Franco, J. S. Blazquez, B. Ingale, and A. Conde, The magnetocaloric effect and magnetic refrigeration near room temperature : materials and models Annu. Rev. Lett. **42**, 305 (2012).

[123] V. K. Pecharsky and K. A. Gschneider, Jr., Giant magnetocaloric effect in $Gd_5(Si_2Ge_2)$ Phys. Rev. Lett. **78**, 4494 (1997).

[124] A. V. Svalov, V. O. Vaskovskiy, A. Larranaga, and G. V. Kurlyandskaya, EPJ Web Conf. **40**, 8005 (2013).

[125] P. Lampen, N. S. Binghan, M. H. Phan, H. Kim, M. Osofsky, A. Pique, T. L. Phan, S. C. Yu, and H. Srikanth, Impact of reduced dimensionality on the magnetic and magnetocaloric response of $La_{0.7}Ca_{0.3}MnO_3$ Appl. Phys. Lett. **102** (6), 062414 (2013).

[126] A. V. Svalov, V. O. Vaskovskiy, J. M. Barandiaran, K. G. Balymov, I. Orue, and G. V. kurlyandskaya, Structure and magnetic properties of nanostructured GdTb Phys. Status. Solidi A **208**, 2273-2276 (2011)

[127] S. P. Mathew and S. N. Kaul, Tuning magnetocaloric effect with nanocrystallite size Appl. Phys. Lett. **98**, 172505 (2011)

[128] B. J. Kirby, J. W. Lau, D. V. Williams, C, A. Bauer, and C. W. Miller, Impact of interfacial magnetism on magnetocaloric properties of thin film heterostructures J. Appl. Phys. **109**, 063905 (2011)

[129] C. H. Lambert, M. S. EL Hadri, M. Hamedoun, A. Benyoussef, O. Mounkachi, and S. Mangin, Tunable magnetocaloric effect in $Gd_{1-x}Tb_x$ heterostructures thin film J. Magn. Magn. Mater. **433**, 1-3 (2017)

[130] R. L. Hadimani, J. H. B. Silva, A. M. Pereira, D. L. Schlagel, T. A. Lograsso, Y. Ren, X Zhang, D. C. Jiles, and J. P. Arajo, Gd5(Si,Ge)4 thin film displaying large magnetocaloric and strain effects due to magneto structural transition Appl. Phys. Lett. **106**, 032402 (2015).

[131] L. M. Moreno-Ramirez, J. S. Blazquer, V. Franco, A, Conde, M. Marsilius, V. Budinsky, and G. Herzer, A new method for determining the Curie temperature from magnetocaloric measurements IEEE Magn. Lett. **7**, 6102004 (2016).

[132] B. K. Banerjee, On a generalized approach to first and second order magnetic transitions Phys. Lett. **12**, 16 (1964).

[133] M. Balli, D. Fruchart, D. Gignoux, S. Miraglia, E. K. Hlil and P. Wolfers, Modelling of the magnetocaloric effect in $Gd_{1-x}Tb_x$ and MnAs compounds J. MAgn. Magn. Mater. **316**, 558-561 (2007).

[134] M. Manekar and S. B. Roy, Reproducible room temperature giant magnetocaloric effect in Fe-Rh J. Phys. D: Appl. Phys. **41**, 192004 (2008).

[135] D. H. Mosca, F. Vidal, and V. H. Etgens, Strain engineering effect in MnAs epilayers Phy. Rev. Lett. **101**, 125503 (2008).

[136] Z. W. Wang, P. Yu, Y. T. Cui, and L. Xia, Near room temperature magneto-caloric effect of a $Gd_{48}Co_{52}$ amorphous alloy J. Alloys Compd. **658**, 598 (2016).

[137] V. S. Kumar, R. Chukka, Z. Chen, P. Yang, and L. Chen, Strain dependent magnetocaloric effect in $La_{0.67}Sr_{0.33}MnO_3$ thin films AIP Adv. **3**, 52127 (2013).

[138] M. Oumezzine, A, C. Galca, I. Pasuk, C. Chirila, A. Leca, V. Kuncser, L. C. Tanase, A. Kumcser, C. Ghica, and M. Oumezzine, Structural magnetic and magnetocaloric effects in epitaxial $La_{0.67}Ba_{0.33}Ti_{0.02}Mn_{0.98}O_3$ ferromagnetic thin films grown on 001-oriented $SrTiO_3$ substrates Dalton Trans. **45**, 15034-15040 (2016)

[139] Q. Zhang, S. Thota, F. Guillou, P. Padhan, V. Hardy, A. Wahl, and W. Prellier, magnetocaloric effect and improved relative cooling power in ($La_{0.7}Sr_{0.3}MnO_3$/$SrRuO_3$) superlattices J. Phys, Condens. Matter **23** (5), 052201 (2011).

[140] C. W. Miller, D. V. Williams, N. S. Bingham, and H. Srikanth, Magnetocaloric effect in Gd/W thin film heterostructures J. App. Phys. **107**, 09A903 (2010).

[141] C. L. Zhnag, D. H. Wanga, Z. D. Han, H. C. Xuan, B. X. Gu, and Y. W. Du, Large magnetic entropy changes in Gd-Co amorphous ribbons J. Appl. Phys. **105**, 013912 (2009).

[142] H. F. Kirby, D. D. Belyea, J. T. Willman, and C. W. Miller, Effects of preparation conditions on the magnetocaloric properties of Gd thin films J. Vac. Sci. Technol. A **31**, 031506 (2013).

[143] D. T. Morelli, A. M. Mance, J. V. Mantese, and A. L. Micheli, Magnetocaloric properties of doped lanthanum manganite films J. App. Phys. **79**, 373 (1996).

[144] D. D. Belyea, T. S. Santos, and C. W. Miller, Magnetocaloric effect in epitaxial $La_{0.56}Sr_{0.44}MnO_3$ Alloy and digital heterostructures J. Appl. Phys. **111**, 07A935 (2012)

[145] V. Recarte, J. I. Perez-Landazabal, V. Sanchez-Alarcos, V. A. Chernenko, and M. Ohtsuka, Magnetocaric effect linked to the martensitic transformation in sputter-deposited Ni-Mn-Ga thin films Appl. Phys. Lett. **95**, 141908 (2009).

[146] V. Provenzano, A. J. Shapiro, and R. D. Shull, Nature London **429**, 853 2004.

[147] P. Hansen, C. Clausen, G. Much, M. Rosenkranz, and K. Witter, J. Appl. Phys. 66, 756 1989.

[148] X. Y. Liu, J. A. Barclay, R. B. Gopal, M. Földeàki, R. Chahine, T. K Bose, P. J. Schurer, and J. L. LaCombe, J. Appl. Phys. 79, 1630 1996.

[149] C. Zimm, A. Jastrab, A. Sternberg, V.K. Pecharsky, K.A. Gschneidner Jr., M. Osborne, I. Anderson, Adv. Cryog. Eng. 43 (1998) 1759–1766.

[150] J. Glanz, Science 279 (1998) 2045.

[151] V.K. Pecharsky, K.A. Gschneidner Jr., Phys. Rev. Lett. 78 (1997) 4494.

[152] V.K. Pecharsky, K.A. Gschneidner Jr., Appl. Phys. Lett. 70 (1997) 24.

[153] K.A. Gschneidner Jr., V.K. Pecharsky, J. Appl. Phys. 85 (1999) 5365.

[154] V.K. Pecharsky, K.A. Gschneidner Jr., J. Magn. Magn. Mater. 200 (1999) 44.

[155] K.A. Gschneidner Jr., V.K. Pecharsky, Ann. Rev. Mater. Sci. 30 (2000) 387.

[156] K.A. Gschneidner Jr., V.K. Pecharsky, A.O. Tsokol, Rep. Prog. Phys. 68 (2005) 1479–1539. [9] E. Warburg, Ann. Phys. 13 (1881) 141.

[157] P. Debye, Ann. Phys. 81 (1926) 1154.

[158] W.F. Giauque, J. Am. Chem. Soc. 49 (1927) 1864.

[159] S.Yu. Dan'kov, A.M. Tishin, V.K. Pecharsky, K.A. Gschneidner Jr., Phys. Rev. B 57 (1998) 3478.

[160] J. Tusek, A. Kitanovski, S. Zupan, I. Prebil, A. Poredos, Appl. Therm. Eng. 53 (1) (2013) 57–66.

[161] A.V. Svalov, V.O. Vas'kovskiy, J.M. Barandiaran, K.G. Balymov, I. Orue, G.V. Kurlyandskaya, Phys. Status Solidi A 208 (2011) 2273–2276.

[162] S.P. Mathew, S.N. Kaul, Appl. Phys. Lett. 98 (2011) 172505.

[163] C.W. Miller, D.V. Williams, N.S. Bingham, H. Srikanth, J. Appl. Phys. 107 (2010) 09A903. [17] B.J. Kirby, J.W. Lau, D.V. Williams, C.A. Bauer, C.W. Miller, J. Appl. Phys. 109 (2011) 063905.

[164] G.I. Kataev, M.R. Sattarov, A.M. Tishin, Phys. Status Solidi A 114 (1989) K79.

[165] D.E. Hegland, S. Legvold, F.H. Spedding, Phys. Rev. 131 (1963) 158.

[166] M. Balli, D. Fruchart, D. Gignoux, S. Miraglia, E.K. Hlil, P. Wolfers, J. Magn. Magn. Mater. 316 (2007) 558–561.

[167] D.M.S. Bagguley, J.P. Partington, J.A. Robertson, R.C. Woods, J. Phys. F: Metal. Phys. 10 (1980) 967–983.

[168] X. Moya, S. Kar-Narayan, N.D. Mathur, Nat. Mater. 13 (2014) 439–450.

[169] S.K. Giri, P. Dasgupta, A. Poddar, R.C. Sahoo, D. Paladhi, T.K. Nath, Appl. Phys. Lett. 106 (2015) 023507. [

[170] K.W. Zhou, Y.H. Zhuang, J.Q. Li, J.Q. Deng, Q.M. Zhu, Solid State Commun. 137 (2006) 275–277.

[171] H.F. Kirby, D.D. Belyea, J.T. Willman, C.W. Miller, J. Vac. Sci. Technol. A 31 (2013) 031506.